

MAGNETO-TRANSPORT AND MAGNETO-OPTICAL PROPERTIES OF FERROMAGNETIC (III,Mn)V SEMICONDUCTORS: A REVIEW

Jairo Sinova,¹ T. Jungwirth,^{2,3} and John Černe⁴

¹*Texas A&M University, Physics Department, 4242 TAMU, College Station, TX 77943-4242*

²*University of Texas at Austin, Physics Department,*

1 University Station C1600, Austin TX 78712-0264

³*Institute of Physics ASCR, Cukrovarnická 10, 162 53 Praha 6, Czech Republic*

⁴*Department of Physics, University at Buffalo, SUNY, Buffalo, New York 14260*

(Dated: October 29, 2018)

Rapid developments in material research of metallic ferromagnetic (III,Mn)V semiconductors over the past few years have brought a much better understanding of these complex materials. We review here some of the main developments and current understanding of the bulk properties of these systems within the metallic regime, focusing principally on the magneto-transport and magneto-optical properties. Although several theoretical approaches are reviewed, the bulk of the review uses the effective Hamiltonian approach, which has proven useful in describing many of these properties namely in (Ga,Mn)As and (In,Mn)As. The model assumes a ferromagnetic coupling between Mn d-shell local moments mediated by holes in the semiconductor valence band.

PACS numbers:

Contents

I. INTRODUCTION

I. Introduction	1	The artificial marriage of ferromagnetic and semiconducting properties is one of the main motivations behind the creation and study of diluted magnetic semiconductors (DMS) focused on (III,Mn)V materials. This effort is being fueled, in large part, by the endless demand for technological advances in our society whose global interdependence in communications and technology is evident throughout our daily activities. Moore's law, predicting an exponential growth of computational ability, is now believed to be in perill and there is a need for a new technological revolution if the fast pace of technology is to be maintained.
A. The basic picture of DMS	2	
B. Impurities in DMS	2	
C. Other experimental observations in DMS	3	
II. Theoretical models of DMS	3	Such a technological revolution will take place if three major goals can be achieved in the development of ferromagnetic (III,Mn)V materials: i) room temperature ferromagnetism, ii) dependence of transport and optical properties on the magnetic state, and iii) that the materials maintain their fundamental semiconducting characteristics, i.e. strong sensitivity to doping, external fields, and light, and are compatible and integrable with conventional (non-magnetic) micro- and opto-electronic semiconductor technologies. Since the first observation of ferromagnetism at low temperatures in the (III,Mn)V semiconductors in the early nineties, ¹ steady progress has been taking place in each of these major fronts. More importantly, over the last five years, jumpstarted by the discovery of ferromagnetism in (Ga,Mn)As with ferromagnetic temperatures in excess of 100 K, ² the efforts in this field have increased dramatically in several coordinated fronts, both experimental and theoretical. This rapid research has yielded many advances, prompting the need for an overall review of at least several fast evolving parts of this scientific effort. In this article we discuss transport and magneto-optical properties of these materials focusing on the metallic regime and on theoretical
III. Transport properties of DMS systems	5	
A. General features of resistivity in DMS	5	
B. Scattering off the kinetic-exchange potential in the paramagnetic regime	5	
C. Boltzman transport theory of the zero temperature conductivity in DMS	6	
D. Hall resistivity and the Anomalous Hall effect	8	
1. The embroiled history of the anomalous Hall effect	8	
2. Anomalous Hall effect in DMS	10	
IV. Optical properties of DMS	12	
A. visible and infrared absorption	12	
1. Multiband effective Hamiltonian approach	12	
2. Lattice models and dynamical mean field theory approach	13	
B. Magneto-optical effects	14	
V. Summary	16	
Acknowledgements	17	
References	17	

cal approaches based on the effective Hamiltonian model which have been successful in obtaining qualitative and quantitative understanding of various transport characteristics of these systems. Other important areas, such as the insulating low-doping regime have been covered by other reviews.^{3,4} Furthermore, we will narrow our focus on the most widely studied and well understood materials, (Ga,Mn)As and (In,Mn)As, only mentioning briefly some of the current prevailing ideas in regards to the much lesser understood ones such as the Mn-doped nitrides or phosphides.

As in any review, a preference must be given to the more relevant publications containing the most recent developments and the ones which have had the largest impact in understanding these complex materials. Unless the reference section is equal in length to the actual review, it is impossible to cite every contribution to this field. To remedy omissions that may have partly originated from the authors' own work perspective, we refer to a more extended and precise database of published and pre-print works maintained within the "Ferromagnetic Semiconductors Web Project" at <http://unix12.fzu.cz/ms>. This web page contains a large body of theoretical and experimental results (that can be obtained in several formats), as well as the most extended bibliography database linked to diluted magnetic (III,V) semiconductors that we are aware of. We encourage the reader in need of a more detailed bibliography to use this resource.

We also note that a few review articles on other aspects of the physics of DMS, which we will not discuss extensively in this review, have appeared over the past few years and may help the reader who wants to extend the narrow scope of this article. Given however the rapid developments over the past two years alone, the reader should be warned that these reviews, although excellent, may not suffice to give the most current experimental developments and theoretical understanding and justifications. Several extended papers on the physics of ferromagnetism and proposed mechanisms, some of which we briefly review here, are shown in Refs. 2,5–7. A theoretical review of the widely used phenomenological Zener mean field model, highly successful in (Ga,Mn)As and (In,Mn)As studies, is presented in Ref. 8 and 9. A large body of work up to 2001 in density functional first principles calculations in (III,V) DMS is also available in Ref. 10. Another theoretical approach based on lattice models and dynamical mean field treatment of disorder, most successful in the low-doping regime, is reviewed in Ref. 3. The ever important effects of disorder, omnipresent in these materials, is reviewed in Ref. 4. A general discussion behind the technological motivation for DMS has been presented in 11, 12, 13, and 14, where optical insulators and magnetoresistance elements are explored.

We organize the rest of this article as follows: In Sec. IA we present a short general overview of DMS from the experimental facts point of view. In Sec. II we briefly

discuss the theoretical model used and its experimental basis to describe the metallic regime. Sec. III reviews the transport properties of DMS such as diagonal resistivity, magneto-resistance anisotropy, and anomalous Hall effect. Sec. IV covers the different optical and magneto-optical properties of the systems such as optical absorption, magnetic-circular dichroism, Raman scattering, and cyclotron resonance. A short summary and outlook with different open questions is given in section V.

A. The basic picture of DMS

The basic idea behind creating these novel ferromagnetic materials is simple: based on the lower valence of Mn, substituting Mn in a (III,V) semiconductor for the cations can dope the system with holes; beyond a concentration of 1% there are enough induced holes to mediate a ferromagnetic coupling between the local $S = 5/2$ magnetic moments provided by the strongly localized $3d^5$ electrons of Mn and a ferromagnetic ordered state can ensue. This rudimentary but generally correct picture of ferromagnetism in many (III,Mn)V materials is of course acquired by peacing together the different experimental results obtained through different characterization techniques of the materials. The simplicity of the model hides within it a cornucopia of physical effects present in these materials such as metal-insulator transitions, carrier mediated ferromagnetism, disorder physics, magneto-resistance effects, magneto-optical effects, intricate coupled magnetization dynamics, post-growth dependent properties, etc.

In any doped semiconductor, an understanding of its properties must be preceded by a study of the doping impurities. Since, in this case, the Mn impurity dopants provide the local magnetic moments responsible for ferromagnetism and, at the same time, provide the hole carriers which mediate the exchange coupling between the impurities themselves, understanding the nature of the impurities and the different states that they induce is even more fundamental in order to establish a relevant theoretical model.

B. Impurities in DMS

Under equilibrium growth conditions, the solubility of Mn in III-V semiconductor crystals has an upper limit of 0.1 %. Beyond this concentration phase separation and surface segregation takes place. To circumvent this problem, low-temperature molecular beam epitaxy (LT-MBE) technique was applied leading to the first successful growth of InAs and GaAs based DMS.¹ The most common and stable position of Mn in the host semiconductor lattice is on the Ga site.^{15–19}

An important initial question is what is the neutral state of the Ga-substitutional Mn impurity. Experimen-

tally, through electron paramagnetic resonance (EPR) and optical measurements,^{16,20,21} for even very few percentage of Mn (lower by an order of magnitude than the concentration marking the metal-insulator transition) the only impurity level observed is the $d^5\text{-Mn}^{2+}$ ionized state, indicating that indeed the strong localized $3d^5$ electrons with total spin $S = 5/2$ are a good starting point for theoretical models. The corresponding $3d^5$ plus a weakly bound hole neutral state is observed experimentally only within a narrow range of Mn concentrations due to a complete compensation in the low Mn doping regime and due to the Mott insulator-to-metal transition at high doping. Other candidates for the Mn neutral impurity such as $3d^4$ states, important for double-exchange models to be applicable, are not observed experimentally.¹⁶ Furthermore, the itinerant holes originating from the Mn acceptor level have also been observed through photoemission experiments^{22,23} to be associated with the ones of the host semiconductor valence band, i.e. they have As 4p-character, which provides further evidence for the shallow acceptor nature of the substitutional Mn impurity in GaAs and InAs.

The other impurities present because of the non-equilibrium growth process, As-antisites and Mn-interstitials, compensate the induced holes and therefore reduce the free carrier concentration with respect to the substitutional-Mn density. Annealing procedures, at temperatures slightly lower than growth temperature, have shown a reduction of the amount of compensation.^{5,24–29} The initial procedure⁵ has now been modified by different groups^{24–26,29} and the carrier concentration can actually be tuned precisely through resistance-monitored annealing.²⁴ Two possible mechanisms for the reduction of compensation have been considered: either the number of As-antisites is reduced through migration of As atoms to their correct sites, or the Mn-interstitials migrate to the surface or to the substitutional sites. Early theoretical models assumed the former scenario, however, a recent key Rutherford backscattering experiment²⁵ has shown that it is the reduction of Mn-interstitials and their out-diffusion to the surface²⁸ which is responsible for lowering the amount of compensation.

C. Other experimental observations in DMS

Besides the experimental results revealing what is happening in the complicated annealing process and the nature of the impurities, there are other experimental observations that provide key clues for understanding the origins and fundamental properties of (Ga,Mn)As and (In,Mn)As DMS:

a) The ferromagnetic behavior of DMS materials is only observed above a critical doping level of about 1%.⁵ At lower doping the compensation is almost complete and the mediating carriers needed to exchange-couple the localized Mn moments are not present and therefore no

ferromagnetic ordering occurs.

b) The carrier-induced ferromagnetic nature of the ordered state has been demonstrated by field-effect (In,Mn)As experiments³⁰ where the carrier concentration was tuned by a gate and the corresponding critical temperature was modified accordingly.

c) Strain effects, due to the lattice mismatch between the DMS layer and the substrate, influence the magnetic anisotropy of the ferromagnetic state. It has been shown that the ferromagnetic easy axis can be along the growth direction or in the plane depending on whether the strain is tensile or compressive.^{5,9} Such phenomena are interpreted in terms of well known strain effects in the spin-orbit coupled valence bands of the host semiconductor.

c) Both magneto-optical effects, e.g. magnetic circular dichroism (MCD),³¹ and resistivity measurements above the critical temperature,³² indicate an antiferromagnetic coupling between the local $3d^5$ electrons and the valence hole. This so-called kinetic-exchange interactions originates from the hybridization between the Mn 3d-orbitals and the neighboring As 4p-orbitals and is much larger than the pure Coulomb exchange interaction.³³

e) In transport measurements, a large anomalous-Hall effect (AHE) (see Sec. IIID) completely dominates the low-field off-diagonal resistance coefficient. The strong intrinsic spin-orbit coupling present in the host semiconductor valence band can account for the measured magnitude and sign of the AHE.

There are of course many other relevant experiments which are not highlighted above which must be taken into account. However the interpretation of some or most of them are still being debated, since they seem to depend critically on the annealing procedures and can be interpreted in several ways. The above results are considered to be general and well established and will likely not change in the newly grown samples as the materials development progresses.

II. THEORETICAL MODELS OF DMS

The modeling of a collective behavior of interacting electrons is a complicated task and, in many instances, must be guided by experimental evidence of the low energy degrees of freedom in order to obtain a correct minimal model which will capture the observed effects and will make useful predictions. With this in mind, there are typically three approaches, somewhat complementary, used to describe DMS systems: first principles density-functional theory (DFT) and microscopic tight-binding models, effective Hamiltonian models, and lattice models.

DFT is an important tool for studying microscopic origins of ferromagnetism through calculations of electronic, magnetic, and structural ground-state properties.¹⁰ A local-density-approximation (LDA) of the DFT, combined with disorder-averaging coherent-potential approx-

imation (CPA) or supercell approach, has been used successfully to address physical parameters of (III,Mn)V DMS that are derived from total-energy calculations, such as the lattice constants,³⁴ and formation and binding energies of various defects.^{18,19} However, in Mn-doped DMS, LDA fails to account for strong correlations that suppress fluctuations in the number of electrons in the d-shell. As a result, the energy splitting between the occupied and empty d-states is underestimated which leads to an unrealistically large d-state local DOS near the top of the valence band and to an overestimate of the strength of the sp-d hybridization.^{10,35} This shortcomings have been corrected recently by LDA+U and self-interaction corrected LDA schemes, which account for correlations among Mn 3d electrons, and have been used to obtain more realistic energy spectra and show agreement with the experimental observation that the valence holes have mostly As 4p-character.³⁶

A practical approach, that circumvents some of the complexities of this strongly-correlated many-body problem is the microscopic tight-binding (TB) band-structure theory. Within the model, local changes of the crystal potential at Mn and other impurities are represented by shifted atomic levels. A proper parameterization of these shifts, of the Hubbard correlation potential that favors single occupancy of the localized d-orbitals, the Hund potential forcing the five d-orbital spins to align, and of the hopping amplitudes between neighboring atoms provides correct band gap for the host III-V semiconductor and an appropriate exchange splitting of the Mn d-levels. The TB model is a semi-phenomenological theory, however, it shares the virtue with first principles approaches of treating disorder microscopically. The decoherence of Bloch quasiparticle states or effects of doping and disorder on the strength of the sp-d exchange coupling and effective Mn-Mn interaction are among the problems that have been analyzed using this tool.³⁷⁻³⁹

In the metallic regime, where the largest critical ferromagnetic temperatures are achieved (for doping levels above 1.5%⁴⁰), semi-phenomenological models that are built on Bloch states for the band quasiparticles, rather than localized basis states appropriate for the localized regime,⁴¹ provide the natural starting point for a model Hamiltonian which reproduces many of the observed experimental effects. Recognizing that the length scales associated with holes in the DMS compounds are still long enough, a $\mathbf{k} \cdot \mathbf{p}$ envelope function description of the semiconductor valence bands is appropriate. Since for many properties, e.g. anomalous Hall effect and magnetic anisotropy, it is necessary to incorporate intrinsic spin-orbit coupling in a realistic way, the six-band (or multiple-band, in general) Kohn-Luttinger (KL) $\mathbf{k} \cdot \mathbf{p}$ Hamiltonian that includes the spin-orbit split-off bands is desirable.^{9,42} The approximation of using the KL Hamiltonian to describe the free holes is based primarily in the shallow acceptor picture demonstrated by the experiments¹⁵⁻¹⁷ in (Ga,Mn)As and (In,Mn)As and must be re-examined for any other DMS materials that

this model is applied to.

Besides the KL Hamiltonian parameters of the host III-V compound which have long been established,⁴³ the phenomenological part of the strategy follows from asserting, rather than deriving, the localized nature of the Mn d-orbital moments and from parameterizing the sp-d hybridization by an effective exchange constant J_{pd} . The localization assumption is again verified by electron resonance experiments¹⁵⁻¹⁷ and the value of J_{pd} is obtained from resistivity measurements in the paramagnetic regime³² and MCD measurements.³¹ Hence, the effective Hamiltonian considered within this model is

$$\mathcal{H} = \mathcal{H}_{KL} + J_{pd} \sum_I \mathbf{S}_I \cdot \hat{\mathbf{s}}(\mathbf{r}) \delta(\mathbf{r} - \mathbf{R}_I) + \mathcal{H}_{dis}, \quad (1)$$

where \mathcal{H}_{KL} is the six-band (multiple-band) Kohn-Luttinger (KL) $\mathbf{k} \cdot \mathbf{p}$ Hamiltonian,^{8,9} the second term is the short-range antiferromagnetic kinetic-exchange interaction between local spin \mathbf{S}_I at site \mathbf{R}_I and the itinerant hole spin (a finite range can be incorporated in more realistic models), and \mathcal{H}_{dis} is the scalar scattering potential representing the difference between a valence band electron on a host site and a valence band electron on a Mn site and the screened Coulomb interaction of the itinerant electrons with the ionized impurities.

Several approximations can be used to vastly simplify the above model, namely, the virtual crystal approximation (replacing the spatial dependence of the local Mn moments by a constant average) and the mean field theory description.^{8,9} In the metallic regime, the disorder can be treated by a Born approximation or by more sophisticated, exact-diagonalization or Monte-Carlo methods.⁴⁴⁻⁴⁸ The effective Hamiltonian in Eq. 1 allows to use standard electron-gas theory tools to account for hole-hole Coulomb interactions. This envelope function approximation model is also suitable for studying magnetic semiconductor heterostructures, like superlattices, quantum wells and digitally doped layers.⁴⁹ The validity of such semi-phenomenological Hamiltonian, which does not contain any free parameters, must be confirmed ultimately by experiments. Its accurate description of many thermodynamic and transport properties of metallic (Ga,Mn)As samples, such as the measured transition temperature,^{50,51} the anomalous Hall effect,^{52,53} the anisotropic magnetoresistance,^{44,52} the magneto-crystalline anisotropy,^{42,54} the spin-stiffness⁵⁴, the ferromagnetic domain wall widths,⁵⁵ the magnetic dynamic damping coefficients,⁵⁶ and the magneto-optical properties,^{9,45,57} has proven the merit of this effective Hamiltonian approach.

One has to keep in mind, however, that as any semi-phenomenological model it may fail to capture the correct physics that leads to the ferromagnetic phase in some materials or in a certain range of parameter values. Such models can only be verified by careful comparison with experiments and tested through their predictions and agreement with experiments. For example, Mn-doped nitride and phosphide compounds or in-

ulating DMS samples with low concentration of Mn ions require a theoretical description that goes beyond the picture of the host band quasiparticles that are weakly hybridized with the localized Mn d-electrons. Particularly nitrates are not believed to be well modeled by this semi-phenomenological Hamiltonian since Mn is a deep acceptor in this case and charge fluctuations on the Mn d-levels may play important role.

There has also been theoretical work on (III,Mn)V DMS materials based on a still simpler model where holes are assumed to hop only between Mn acceptor sites, where they interact with the Mn moments via phenomenological exchange interactions.^{3,58} These models have the advantage of approaching the physics of the insulating dilute Mn limit, and can also be adapted to include the holes that are localized on other ionized defects besides the Mn acceptors through dynamical mean field (or CPA) techniques. The free-parameter nature of this phenomenological approach and their oversimplified electronic structure allows to make only qualitative predictions, however, and the models are also not appropriate for studying the high T_c metallic samples.

III. TRANSPORT PROPERTIES OF DMS SYSTEMS

The different transport coefficients of DMS and their magnetic, temperature, and material composition dependence have been the most important and widely used characterization tools of DMS. Besides the diagonal resistivity which indicates metal-insulator transitions and possible critical behavior at the ferromagnetic transition temperature, other material transport properties such as anisotropic magnetoresistance, anomalous and ordinary Hall effect, and giant magnetoresistance have been used to both characterize and test the different theoretical models of DMS materials. In this section we consider the diagonal conductivity general features, how the exchange coupling between the localized moments and free carriers is extracted within the paramagnetic regime, the doping and carrier concentration conductivity dependence at low temperatures, the anisotropic magnetoresistance, and the anomalous Hall effect. Throughout, we will focus on the comparison of theoretical models (mainly the semi-phenomenological effective Hamiltonian model relevant to the metallic regime) to the different experimental observations.

A. General features of resistivity in DMS

DMS materials exhibit an insulating or metallic behavior (defined by the resistivity in the limit of zero temperature) depending on its doping level and post-growth annealing procedures. In as-grown samples, metallic behavior is typically observed for a range of 2-5% Mn doping and an insulating behavior for higher and lower dop-

ing than this range.⁵⁹ In addition to this metal-insulator quantum transition, the resistivity as a function of temperature typically exhibits a peak or shoulder near the ferromagnetic transition temperature for both insulating (peak) and metallic (shoulder) samples.⁵⁹⁻⁶² The non-monotonic behavior near T_c is typically associated with critical-scattering but so far no theory has been developed which explains such behavior in a qualitative or quantitative way. Typically the Fisher-Langer theory of correlated fluctuations is invoked, however, it predicts an infinite derivative of the resistivity at T_c , which is clearly not the case in any studied (Ga,Mn)As DMS sample. There exists also a drastic reduction of the resistivity upon annealing, associated with the increase of the carrier concentration and to a lesser extent a reduction of the disorder scatterers.^{24,59-62} The on-set of the metal-insulator transition at 1.5% Mn doping is close to the Mott insulator limit of a doped semiconductor similar to Si:P and the optimally annealed samples remain metallic throughout the whole range of Mn concentrations above 1.5%.⁴⁰

The number of research groups involved in the materials growth process, each trying a slightly different annealing process, has increased over the past few years and with it a dramatic increase of carrier concentration and conductivity has taken place, as shown in Fig. 1. At the same time the T_c has also increased in accordance with the mean field theory prediction that $T_c \propto xp^{1/3}$, where x is the Mn concentration and p is the carrier concentration. The shoulder in ρ observed in the most recent optimally annealed samples near T_c has been partially explained theoretically in terms of the variation of the Fermi surface and the transport scattering time associated with the ferromagnetic to paramagnetic phase transition.⁶³ However, there is no model at present that reproduces fully the behavior observed in ρ as a function of temperature near T_c in the metallic regime for most samples. There has also been theoretical progress in understanding the low temperature regime⁴⁴ (Sec. III C) and the role of scattering off magnetic impurities in the high temperature paramagnetic regime (Sec. III B).^{32,59}

B. Scattering off the kinetic-exchange potential in the paramagnetic regime

The contribution from magnetic impurities to the resistivity behavior observed above T_c can be understood assuming scattering from the kinetic-exchange term in the Hamiltonian

$$\mathcal{H}_{k-e} = J_{pd} \sum_I \delta(\mathbf{r} - \mathbf{R}_I) \mathbf{S}_I \cdot \mathbf{s}. \quad (2)$$

The corresponding contribution to the resistivity is given by^{32,33}

$$\rho_s = 2\pi^2 \frac{k_F}{pe^2} \frac{(m^*)^2 J_{pd}^2}{h^3} N_{Mn} [2\chi_{\perp}(T, B) + \chi_{\parallel}(T, B)], \quad (3)$$

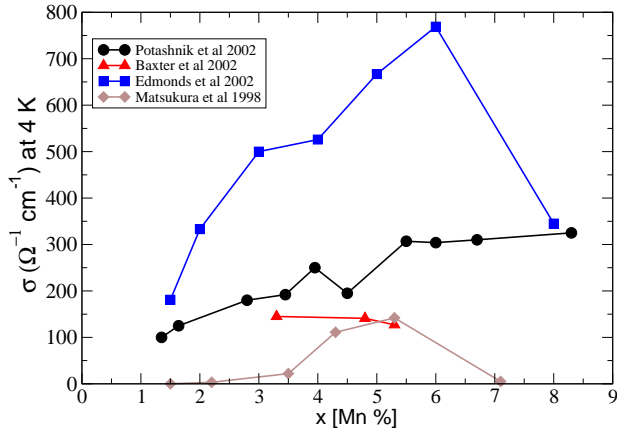


FIG. 1: Conductivity σ measured at 4 K or lower vs. Mn percentage concentration for (Ga,Mn)As. The symbols correspond to: squares to FIX Ref. 24, circles to Ref. 64, triangles to Ref. 65, and dimonds to Ref. 59.

where k_F is the carrier Fermi wave vector, h is the Planck constant, N_{Mn} the density of substitutional Mn, m^* is the effective mass of the carrier, and e is the electron charge. $\chi_{\perp} = M/B$ and $\chi_{II} = \partial M/\partial B$ are the transverse and longitudinal magnetic susceptibilities. Using transport data, the susceptibility can be determined from the Hall resistivity due to the dominant contribution from the anomalous Hall effect which is proportional to the magnetization.³² The analysis of magnetoresistance data above T_c gives $J_{pd} = 55 \pm 10 \text{ meVnm}^3$. This result is in agreement with optical MCD data (see Sec. IV). We also note that the initial expression used to analyze the magnetoresistance data which replaces the susceptibility factor by $[S(S+1) - \langle \mathbf{S} \rangle^2]$, neglected the correlations between neighboring Mn spins and overestimated J_{pd} by a factor of 3 in disagreement then with the MCD measurement of J_{pd} .⁵⁹

C. Boltzman transport theory of the zero temperature conductivity in DMS

The zero temperature conductivity of metallic DMS samples can be obtained from the effective Hamiltonian (Eq. 1) and by accounting for disorder scattering perturbatively. The valence band holes interact with randomly located spins of substitutional Mn impurities via the kinetic-exchange interaction, and with randomly located ionized defects and each other via Coulomb interactions. At zeroth order, the interactions are replaced by their spatial averages, so that the Coulomb interaction vanishes and hole quasiparticles interact with a spatially constant kinetic-exchange field. The corresponding

mean-field Hamiltonian for the itinerant holes reads

$$\mathcal{H}_0 = \mathcal{H}_{KL} + J_{pd} N_{Mn} S \hat{\Omega} \cdot \vec{s}, \quad (4)$$

where $\hat{\Omega}$ is the orientation of fully polarized substitutional Mn local moments and \vec{s} is the envelope-function hole spin operator.⁴² Using the eigenstates of the Hamiltonian in Eq. 4, the first order Born approximation of the elastic scattering rate, and the relaxation-time-approximation solution to the semiclassical Boltzmann equation, the diagonal dc conductivity tensor along one of the cube edges of the host lattice can be written as:⁴⁴

$$\sigma_{\alpha\alpha} = \frac{e^2}{\hbar V} \sum_{n,\vec{k}} \frac{1}{\hbar \Gamma_{n,\vec{k}}} \left(\frac{\partial E_{n,\vec{k}}}{\partial k_{\alpha}} \right)^2 \delta(E_F - E_{n,\vec{k}}), \quad (5)$$

where $\Gamma_{n,\vec{k}}$ is the quasiparticle elastic scattering rate, n and \vec{k} are the band and wavevector indices, $E_{n,\vec{k}}$ are the eigenstates of the Hamiltonian (4), and E_F is the Fermi energy.

The Born approximation estimate of the transport weighted scattering rate from substitutional Mn impurities is given by:

$$\Gamma_{n,\vec{k}}^{Mn} = \frac{2\pi}{\hbar} N_{Mn} \sum_{n'} \int \frac{d\vec{k}'}{(2\pi)^3} |M_{n,\vec{k};n',\vec{k}'}|^2 \times \delta(E_{n,\vec{k}} - E_{n',\vec{k}'}) (1 - \cos \theta_{\vec{k},\vec{k}'}), \quad (6)$$

with the scattering matrix element,

$$M_{n,\vec{k};n',\vec{k}'}^{\vec{k},\vec{k}'} = J_{pd} S \langle z_{n\vec{k}} | \hat{\Omega} \cdot \vec{s} | z_{n'\vec{k}'} \rangle - \frac{e^2}{\epsilon_{host} \epsilon_0 (|\vec{k} - \vec{k}'|^2 + q_{TF}^2)} \langle z_{n\vec{k}} | z_{n'\vec{k}'} \rangle. \quad (7)$$

Here ϵ_{host} is the host semiconductor dielectric constant, $|z_{n\vec{k}}\rangle$ is the six-component (multi-component) envelope-function eigenspinor of the unperturbed Hamiltonian (4), and the Thomas-Fermi screening wavevector $q_{TF} = \sqrt{e^2 \text{DOS}(E_F) / (\epsilon_{host} \epsilon_0)}$, where $\text{DOS}(E_F)$ is the density of states at the Fermi energy.⁴⁴ This model incorporates the fact that the transport properties of these materials are not solely determined by the scattering from substitutional Mn impurities and allows explicitly for scattering from compensating defects, which have been seen to play a key role in the resistivity through the post-growth annealing as discussed earlier.^{5,24-29} As-antisite defects are non-magnetic double-donors and contribute to scattering through a screened charge $Z = 2$ Coulomb potential. The double-donor Mn interstitials^{24,27} are unlikely to be magnetically ordered and can also be modeled as a $Z = 2$ screened Coulomb potential.¹⁹

Assuming a parabolic-band dispersion for majority heavy-hole states the kinetic-exchange scattering contribution to the scattering rate can be estimated by, $\Gamma_{pd} = (N_{Mn}) J_{pd}^2 S^2 m^* \sqrt{2m^* E_F} / (4\pi \hbar^4)$. The Mn and As-antisite Coulomb scattering leads to scattering rate Γ_C

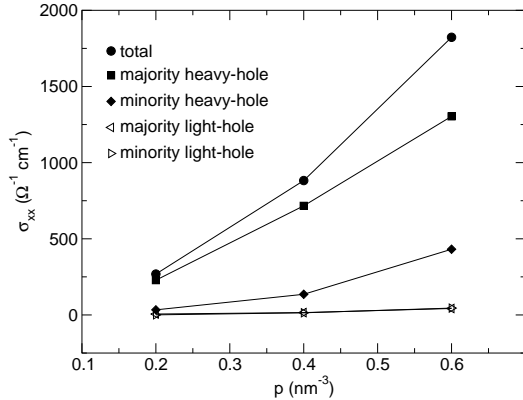


FIG. 2: Conductivity for measuring current and magnetization directed along the x -axis in the plane of the (Ga,Mn)As film as a function of the total hole density. These results were obtained for a GaAs semiconductor host doped with 6% Mn. For typical hole densities the current is carried mostly by the majority heavy-holes.

given by the Brooks-Herring formula.⁴⁴ For (Ga,Mn)As, taking a heavy-hole effective mass $m^* = 0.5m_e$, $p = 0.4 \text{ nm}^{-3}$ and Mn doping $x = 5\%$, these estimates give $\hbar\Gamma_{pd} \sim 20 \text{ meV}$ and $\hbar\Gamma_C \sim 150 \text{ meV}$. A full numerical six-band calculation is consistent with these estimates, and predicts that the Coulomb contribution to the elastic scattering rate is several times larger than the kinetic-exchange contribution for typical chemical compositions. Note that these estimates give an immediate check on the assumption of the theory itself, since even in the heavily doped and compensated (Ga,Mn)As DMS, the lifetime broadening of the quasiparticle ($\hbar\Gamma$) is smaller than the valence band spin-orbit coupling strength ($\Delta_{so} = 341 \text{ meV}$) and the typical Fermi energy.

Fig. 2 shows σ_{xx} , calculated numerically using the six-band Kohn-Luttinger model and Eqs. (5) and (6), for a fully strained $\text{Mn}_{0.06}\text{Ga}_{0.94}\text{As}$ sample. The substrate – DMS lattice mismatch, $e_0 \equiv (a_{sub} - a_{DMS})/a_{DMS}$, is between -0.002 and -0.003 in this case.^{2,65,66} The absolute conductivities predicted by this model are reasonably consistent with experiment.^{24,64,65} The disagreement for lower Mn concentrations ($x < 4\%$) of the theoretical conductivities is most likely due to some combination of inaccuracy in the scattering amplitude estimates, unaccounted sources of scattering, and, especially at small x , coherent scattering effects that eventually lead to localization observed as an upturn in ρ at the lowest temperatures.

In addition to the AHE (Sec. IIID), strong spin-orbit coupling in the semiconductor valence band leads also to anisotropies in the longitudinal transport coefficients. In particular, when the magnetization \mathbf{M} is rotated by applying an external magnetic field stronger than the magneto-crystalline anisotropy field the in-plane

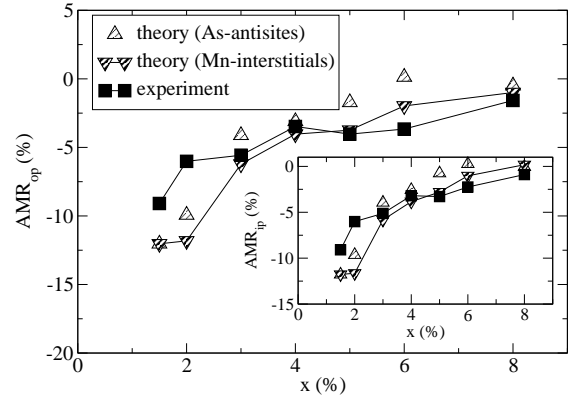


FIG. 3: Experimental (filled symbols) AMR coefficients and theoretical data obtained assuming As-antisite compensation (open symbols) and Mn-interstitial compensation (semi-filled symbols) of AMR_{op} and AMR_{ip} . After Ref. 52

conductivity changes.^{65,67} Fig. 3 shows the theoretical and experimental AMR coefficients, $AMR_{op} = [\sigma_{xx}(\mathbf{M} \parallel \hat{z}) - \sigma_{xx}(\mathbf{M} \parallel \hat{x})]/\sigma_{xx}(\mathbf{M} \parallel \hat{x})$ and $AMR_{ip} = [\sigma_{xx}(\mathbf{M} \parallel \hat{y}) - \sigma_{xx}(\mathbf{M} \parallel \hat{x})]/\sigma_{xx}(\mathbf{M} \parallel \hat{x})$, for the seven (Ga,Mn)As samples.^{24,52,65} Here \hat{z} is the growth direction. Results of the two disordered system models, one assuming As-antisite and the other one Mn-interstitial compensation, are plotted in Fig. 3. As in the AHE case, the theoretical results are able to account semi-quantitatively for the AMR effects in the (Ga,Mn)As DMS, with somewhat better agreement obtained for the model that assumes Mn-interstitial compensation, which confirms indirectly the experimental finding that the compensating defects are dominated by Mn-interstitials.²⁷ Note that although the magnitude of the conductivities tend to be overestimated, the magnetotransport effects are relatively insensitive to scattering strength, reflecting instead the strong spin-orbit coupling in the valence band of the host semiconductor as compared to the Fermi energy.⁵²

A large anisotropic magnetoresistance effect is observed experimentally also in the off-diagonal symmetric conductivity component ($\sigma_{xy} = +\sigma_{yx}$) when magnetization direction changes from parallel to \hat{x} - or \hat{y} -axis, where $\sigma_{xy} = \sigma_{yx} = 0$, to a general orientation in the x - y plane tilted from the two transport measurement axes, where $\sigma_{xy} = \sigma_{yx} \neq 0$.⁶⁸ The effect is called sometimes a 'planar Hall effect' but we emphasize that the true Hall response requires the symmetry $\sigma_{xy} = -\sigma_{yx}$. The anomalous contribution to this asymmetric off-diagonal transport coefficient is discussed in the following section.

D. Hall resistivity and the Anomalous Hall effect

One of the most important characterization tools of magnetic materials is the anomalous Hall effect⁶⁹. The Hall resistance $R_{Hall} \equiv \rho_{xy}/d$ of a magnetic thin film is empirically observed to contain two distinct contributions. The first arises from the normal Hall effect contribution which is proportional to the applied magnetic field, H , and the second, called the anomalous Hall contribution, is observed to be proportional to the magnetization⁷⁰:

$$R_{Hall} = R_0 H + R_S M, \quad (8)$$

where M is the magnetization perpendicular to the thin film surface, and R_0 and R_S are the ordinary and anomalous Hall coefficients respectively. The ordinary Hall effect is due to the Lorentz force on the carriers and is used to measure the concentration and nature of the free carriers since R_0 is linearly proportional to the free carrier density and its sign determines whether they are electrons or holes. On the other hand, the anomalous Hall effect is a direct consequence of the presence of spin-orbit coupling in the system. In many instances, such as the DMS for example, the anomalous contribution is much greater than the ordinary Hall effect, making the carrier density hard to measure since large magnetic field must be used to extract the linearity in the field of the Hall resistance. However, the overwhelming of the Hall coefficient by R_S allows one to utilize the anomalous Hall effect as an indirect measure of the magnetization. Empirically R_S is observed to depend quadratically or linearly on the diagonal resistivity, ρ , depending on the material. For example, for the case of Fe⁷⁰ and GaMnAs⁶⁶ the dependence on the resistivity is quadratic. These two resistivity dependencies of R_S correspond to different possible origins of the anomalous Hall effect which we discuss below. However, in spite of its wide use, it is surprising how much confusion has followed over the past six decades. Although much progress has taken place over the past few years with the creation and study of new materials, no single theory has been able to systematically and convincingly explain the constant puzzle of side-jump vs. intrinsic mechanisms (see below) although it is at present a feasible but challenging undertaking.

1. The embroiled history of the anomalous Hall effect

Before discussing the theoretical description of the anomalous Hall effect in DMS, it is appropriate to make an excursion to the history of the field in order to understand clearly the origin of the controversies and the strengths and weaknesses of the different arguments put forth by different researchers. Often such summaries are done in two or three sentences giving an oversimplified view of the controversy and the different points of view, some of which have been challenged in later literature but still remain in the general folklore.

The first detailed theoretical consideration of the anomalous Hall effect was given by Karplus and Luttinger⁷¹, where they considered the problem from a perturbative point of view (with respect to an applied electric field) and obtained a contribution to the Hall conductivity in systems with spin-orbit coupled Bloch states given by the expression (Eq. 2.16 and 2.17 in Ref. 71)

$$\sigma_{xy} = -\frac{2e^2}{\hbar V} \sum_{n, \vec{k}} n_F(E_{\vec{k}, n}) \text{Im} \left\langle \frac{\partial u_{n, \vec{k}}}{\partial k_y} \left| \frac{\partial u_{n, \vec{k}}}{\partial k_y} \right. \right\rangle, \quad (9)$$

where n_F is the Fermi occupation number of the Bloch state $|u_{n, \vec{k}}\rangle$. This expression is obtained by ignoring impurity scattering (i.e. clean limit) and can also be obtained from the Kubo linear response theory in this clean limit (see below). One of its immediate successes was the prediction that R_S is proportional to ρ^2 in agreement with many materials, Fe being the primary example. Immediately after Karplus and Luttinger's pioneer work, Smit⁷² considered the problem of impurity scattering within a Boltzman formalism using a model Hamiltonian of an electron gas, i.e. plain waves, without intrinsic spin-orbit coupling and a scattering potential containing both direct and spin-orbit coupled terms:

$$\mathcal{H} = \frac{\hat{p}^2}{2m} + V(r) + \frac{1}{2m^2 c^2 r} \frac{\partial V(r)}{\partial r} \hat{S}_z \hat{L}_z \quad (10)$$

where the impurity potential is $V(r) = 0$ for $r > R$ and $V(r) = V_0$ for $r < R$. Within the Boltzman formalism, he obtained a second type of contribution to the Hall conductivity due to the asymmetric scattering from impurities originating from the spin-orbit coupling term. This so called skew-scattering mechanism predicts, in contrast to the intrinsic effect found by Karplus and Luttinger, that $R_S \propto \rho$ (i.e. density of scatterers) and depends on the type and range of the scattering potential. It was also noted that the magnitude of the effect within such simplified model was many orders of magnitude lower than the observed magnitude of the AHE but, as it was shown later, the origin of this deficiency is the lack of intrinsic spin-orbit coupling present in the crystal Bloch states. However, Smit also criticized Karplus and Luttinger's result claiming the intrinsic contribution vanishes. Such claim (see below) is now understood to be unjustified but has remained lingering in the AHE literature, generating much confusion.

Karplus and Luttinger⁷¹ did not consider impurity scattering, hence omitted the skew-scattering contribution in their calculation. To remedy this, Kohn and Luttinger⁷³ developed a consistent (and somewhat cumbersome) treatment to obtain the transport coefficients in the presence of spin-orbit coupling and disorder scattering based on a density matrix expansion. Such approach is equivalent to the Kubo linear response formalism but technically more difficult when applied to real physical systems. Within this formalism the expansion

is done to first order in spin-orbit coupling and impurity scattering strengths. They obtained, besides the previous Karplus and Luttinger result (Eq. 135 in Ref. 73, however note that it has the wrong sign later corrected in Ref. 74), formal expressions for additional contributions due to impurity scattering. Applying this formalism to a model with uncorrelated impurity potential and small scattering strength, Luttinger⁷⁴ obtained, besides the Smit's skew-scattering term, the same final expression as Karplus and Luttinger *but* with the opposite sign (Eq. 3.26 in Ref. 74). Somehow, in addition to the intrinsic Karplus and Luttinger term, there seemed to be an additional contribution from scattering *in the high mobility limit* giving a contribution identical to the intrinsic one but with a factor of -2 in front of it, hence the flip of sign of the final expression. No explanation was given of why such a scattering contribution *does not* depend in any way on the scattering potential but simply on the electronic structure of the system. However, Luttinger⁷⁴ showed unequivocally that the cancelation argued by Smit does not take place. In a slightly different formalism Adams and Blouht⁷⁵ agreed with Luttinger's results and pointed out that Smit's error occurs from an inconsistency involving a change of representation of his density matrix when calculating the current.

A few years later Berger⁷⁶ made his first contribution to the problem introducing the idea (contained within Luttinger's formalism) of the side-jump scattering mechanism. He considered the problem of wave-packet scattering off an impurity potential as in Eq. 10, showing that in addition to skew scattering there exists a side-step type of scattering. This so called side-jump, as in the Luttinger formalism, was independent of the scattering potential, leaving one with the strange notion that an extrinsic scattering mechanism resulted in an intrinsic property. After putting this contribution in a Boltzman type of formalism he obtained a result which was four orders of magnitude lower than the Karplus and Luttinger intrinsic result. He then argued that the intrinsic spin-orbit coupling of the system increases this side-jump scattering by such factor. In his case the sign of the effect is not directly considered and his result, as already mentioned, is independent of the scattering potential itself. A similar type of formalism was put forth by Lyo and Holstein⁷⁷ claiming similar results but ignoring, for some unknown reason, intrinsic non-vanishing contributions of Karplus and Luttinger.

It is then that Leroux-Hugon and Ghazali⁷⁸ pointed out the resolution of the missing order of magnitude of the skew-scattering. By looking simply at scattering of Bloch electrons from ionized impurities $V_{ion}(r)$ alone and going to second order in the Born approximation within the collision term of the Boltzman transport theory, they obtained a skew-scattering contribution with a much higher magnitude than the one coming from the spin-orbit coupling of the impurities themselves. Hence, it became evident that it is the presence of *intrinsic* spin-orbit coupling through the crystal potential which is ul-

timately responsible for the magnitude of all the anomalous Hall effect contributions observed and a system with weak or no intrinsic spin-orbit coupling will not exhibit a detectable contribution to the R_{Hall} .

To elucidate this confusing and farraginous atmosphere, Nozieres and Lewiner⁷⁹, following the formalism introduced by Fivaz⁸⁰ in terms of effective Hamiltonians of semiconductors, developed a theory applicable to narrow gap semiconductors equivalent to Luttinger's⁷⁴ but with the final result in being more physically transparent. Going to linear order in impurity scattering and spin-orbit coupling and combining them with a Boltzmann type of approach, they obtained different contributions to the Hall current and different behavior when considering opposite orders of limits of $\omega \rightarrow 0$ and $\tau \rightarrow \infty$, where ω is the frequency of the applied electric field and τ is the quasiparticle lifetime (see Table I and Eqs. 59, 60a, and 60b in Ref. 79). Besides the skew scattering contribution which depends on the type of scattering potential, in the limit $\omega\tau \gg 1$ ($\tau \rightarrow \infty$ first), considered by some authors to be the weak scattering limit (see Refs. 81 and 82), the result is that of Karplus and Luttinger.⁷¹ On the other hand, for $\omega\tau \ll 1$ ($\omega \rightarrow 0$ first), the opposite sign expression of Luttinger⁷⁴ is recovered. One must note however that this result seems to be very specific to the model (single band) and to the meaning of the limit $\tau \rightarrow \infty$ as admitted by the authors themselves.^{74,79}

After this Berger and Smit exchanged salvos in a series of confusing comments⁸³⁻⁸⁶ in which Smit's old argument, that there is no such a thing as side-jump or intrinsic contribution, seems to have been finally put to rest. It was after this that Chazalviel⁸¹, using Nozieres-Lewiner-Luttinger^{74,79} and Leroux-Hugon and Ghazali's⁷⁸ results, attempted to compare phenomenologically the AHE theory to n-InSb and n-Ge experimental data with some success. Within such models, the relative importance of the side-jump/intrinsic contribution $\sigma_{aH}^{sj/int}$ (which are the same magnitude but of opposite sign depending on the limits^{79,81,82}) to the skew-scattering contribution σ_{aH}^{sk} depends on the nature of the scatterers (only through the skew-scattering dependence). For scattering from ionized impurities one has^{78,81}

$$\left| \frac{\sigma_{aH}^{sj/int}}{\sigma_{aH}^{sk}} \right| = \frac{cN}{pr_s k_F l}, \quad (11)$$

with N/p being the ratio of the total number of ionized impurities and carrier density, r_s is the average distance between carriers in units of Bohr radius, l is the mean free path, and $c \sim 10$, varying slightly with scattering length. For short range scattering potential considered by Luttinger⁷⁴ and Nozieres and Lewiner⁷⁹, $V(\vec{r}) = V_0 \delta(\vec{r} - \vec{r}_i)$:

$$\left| \frac{\sigma_{aH}^{sj/int}}{\sigma_{aH}^{sk}} \right| = \frac{3}{\pi |V_0| D(E_F) k_F l}, \quad (12)$$

where $D(E_F)$ is the density of states at the Fermi energy and k_F is the Fermi wave-vector. These estimates can be

a useful first guess at which mechanism dominates in different materials but one must keep in mind the simplicity of the models used to estimate such ratio.

In spite of the theory being incomplete, and in some cases self-contradictory and puzzling, the theoretical developments remained somewhat dormant until recent interest in new ferromagnetic and spintronic materials. These emerging field have demonstrated the need for a better theoretical understanding of the AHE which has constantly been used to characterize ferromagnetic materials.

We emphasize that there is, at this stage, no controversy regarding the skew-scattering contribution. In most materials such contribution, although present, is minor and in most ferromagnetic materials the quadratic dependence of R_S is observed even at the lowest temperatures. However, if somehow, one could artificially turn down ρ one would eventually reach a regime where such contribution is dominant, a fact which very few people dispute since the origin of such contribution is rather transparent and reassuringly extrinsic in nature. However, the flip of sign of the expressions derived by Luttinger⁷⁴ and Nozieres and Lewer⁷⁹ within the simple one band model in the different order of limits of $\omega\tau$, remains quite disturbing and a source of continuous debates. After all, these results are only obtained in a limit where, supposedly, the skew scattering would always dominate. As we will see below, it seems that in many materials experimental comparisons, the ultimate test of validity of any theory, are more consistent with the intrinsic Karplus and Luttinger⁷¹ contribution than the reversed sign one of Luttinger⁷⁴; the sign of the effect being a simple thing to check.

A possible resolution to the problem would be to perform the Hall conductivity calculation within the Kubo linear response formalism, treating disorder and spin-orbit coupling on an equal footing. This can be achieved by starting from the Dirac representation and taking the weak relativistic limit after treating disorder in the usual fashion. In this way, any spin-orbit coupling contribution comes naturally from the Dirac representation and therefore is automatically taken into account. On the other hand, if one starts from the Pauli Hamiltonian, an immediate question arises: which vertex corrections capture the different contributions to the anomalous Hall effect? Such an approach was taken recently by Crepieux, Dugaev, and Bruno.⁸⁷⁻⁸⁹ The work considers, however, a free electron gas model rather than a crystalline environment, hence ignoring the intrinsic spin-orbit coupling effects. In spite of this simplification, the authors obtained many useful findings. They were able to pinpoint which diagrams correspond to the skew and the side-jump scattering in the Pauli Hamiltonian by identifying them from the corresponding ones arising naturally from the Dirac formalism. Notably, these diagrams within the Pauli Hamiltonian, are not the standard ones that one would take into account naturally. Their main result, Eq. 50 and 51 in Ref. 87,89, is in reasonable agreement with Berger's simpler treatment of this free

electron gas problem.

Taking into consideration the confusion generated by the possible relevance of the side-jump scattering mechanism, several researchers have chosen to focus instead on the original intrinsic contribution to the AHE proposed by Karplus and Luttinger⁷¹ and ignore impurity scattering all together or simply include its effects through the Born approximation which introduces a finite quasiparticle lifetime. In DMS, e.g., this approach is partly motivated by the strong intrinsic spin-orbit coupling in the host valence bands that makes much of the above theoretical discussions inapplicable since they relied on the perturbation treatment of the spin-orbit coupling. One of the main attraction of the intrinsic AHE theory is the ability to do calculations in models with realistic electronic band-structures. This approach has been used, e.g., to analyze the AHE in layered 2D ferromagnets such as SrRuO₃, in pyrochlore ferromagnets⁹⁰⁻⁹³, in the colossal magnetoresistance manganites,⁹⁴ in Fe,⁹⁵ in DMS,⁵³ and as a natural starting point to address infrared magneto-optical effects such as the Kerr and Faraday effects⁵⁷ (see Sec. V). The application of this approach to these different materials and their successful comparison to experiments^{52,53,66,90-92,95,96} is perhaps the most poignant criticism to the old theories regarding the side-jump scattering as fundamental.

2. Anomalous Hall effect in DMS

The anomalous Hall effect in DMS has been one of the most fundamental characterization tools since it is the simplest way of detecting the ferromagnetic state of the system at a given temperature. The original discovery of ferromagnetism in (III,Mn)V semiconductors was established by measuring the AHE in both the high and low temperature regimes.¹ The comparison with remanent magnetization measurements using a SQUID magnetometer confirmed, e.g., that AHE measurement can be used to determine ferromagnetic critical temperature.¹

Recently Jungwirth, Niu, and MacDonald⁵³ reintroduced the original Karplus and Luttinger Eq. 9, pointing out that the intrinsic contribution to the AHE is proportional to the Berry phase acquired by a quasiparticle wave function upon traversing closed path on the spin-split Fermi surface. They applied the theory to metallic (III,Mn)V materials using both the 4-band and 6-band $\vec{k}\cdot\vec{p}$ description of the valence band electronic structure⁴² and obtained results in a quantitative agreement with the experimental data in (Ga,Mn)As and (In,Mn)As DMS. In DMS systems, the estimate given in Eq. 11 gives a ratio of intrinsic to skew scattering contribution of the order of 50, hence the intrinsic contribution in these systems is likely to dominate.⁸² Consistently, Edmonds *et al.*⁹⁶ found that in metallic DMS systems $R_s \propto \rho^2$. In a follow up work⁵² a more careful comparison of the theory, reformulated within the Kubo formalism, was done in order to

account for finite quasiparticle lifetime effects important only for quantitative but not qualitative comparison with the experimental data. Within the Kubo formalism the dc Hall conductivity for non-interacting quasiparticles is given by

$$\sigma_{xy} = \frac{ie^2\hbar}{m^2} \int \frac{d\vec{k}}{(2\pi)^3} \sum_{n \neq n'} \frac{f_{n',\vec{k}} - f_{n,\vec{k}}}{E_{n\vec{k}} - E_{n'\vec{k}}} \times \frac{\langle n\vec{k} | \hat{p}_x | n'\vec{k} \rangle \langle n'\vec{k} | \hat{p}_y | n\vec{k} \rangle}{E_{n'\vec{k}} - E_{n\vec{k}} + i\hbar\Gamma}. \quad (13)$$

Looking at the real part of the dc Hall conductivity in the clean limit ($\hbar\Gamma \rightarrow 0$), the delta-function contribution from the denominator vanishes due to the Fermi factor differences and we obtain

$$\sigma_{xy} = \frac{e^2\hbar}{m^2} \int \frac{d\vec{k}}{(2\pi)^3} \sum_{n \neq n'} (f_{n',\vec{k}} - f_{n,\vec{k}}) \times \frac{\text{Im}[\langle n'\vec{k} | \hat{p}_x | n\vec{k} \rangle \langle n\vec{k} | \hat{p}_y | n'\vec{k} \rangle]}{(E_{n\vec{k}} - E_{n'\vec{k}})^2}. \quad (14)$$

Realizing that the dipole matrix elements considered above can be written as $\langle n'\vec{k} | \hat{p}_\alpha | n\vec{k} \rangle = (m/\hbar) \langle n'\vec{k} | \partial H(\vec{k}) / \partial \alpha | n\vec{k} \rangle$, Eq. 14 can be shown to be equivalent to Eq. 9. However, within the Kubo formalism, it is straightforward to account for the finite lifetime broadening of the quasiparticles within the simple Born approximation by allowing Γ above to be finite. The effective lifetime for transitions between bands n and n' , $\tau_{n,n'} \equiv 1/\Gamma_{n,n'}$, can be calculated by averaging quasiparticle scattering rates calculated from Fermi's golden rule including both screened Coulomb and exchange potentials of randomly distributed substitutional Mn and compensating defects as done in the dc Boltzman transport studies^{44,45}. In Fig. 4 the compensation is assumed to be due entirely to As-antisite defects. The valence band hole eigenenergies $E_{n\vec{k}}$ and eigenvectors $|n\vec{k}\rangle$ in Eqs. (13)-(14) are obtained by solving the six-band Kohn-Luttinger Hamiltonian in the presence of the exchange field, $\vec{h} = N_{Mn} S J_{pd} \hat{z}$ ⁴². Here $N_{Mn} = 4x/a_{DMS}^3$ is the Mn density in the $\text{Mn}_x\text{Ga}_{1-x}\text{As}$ epilayer with a lattice constant a_{DMS} , the local Mn spin $S = 5/2$, and the exchange coupling constant $J_{pd} = 55 \text{ meV nm}^{-3}$.

Fig. 4 demonstrates that whether or not disorder is included, the theoretical anomalous Hall conductivities are of order $10 \Omega^{-1} \text{ cm}^{-1}$ in the (Ga,Mn)As DMS with typical hole densities, $p \sim 0.5 \text{ nm}^{-3}$, and Mn concentrations of several per cent. On a quantitative level, disorder tends to enhance σ_{AH} at low Mn doping and suppresses AHE at high Mn concentrations where the quasiparticle broadening due to disorder becomes comparable to the strength of the exchange field. The inset in Fig. 4 also indicates that the magnitude of the AHE in both models is sensitive not only to hole and Mn densities but also to the lattice-matching strains between substrate and the magnetic layer, $e_0 = (a_{\text{substrate}} - a_{DMS})/a_{DMS}$.

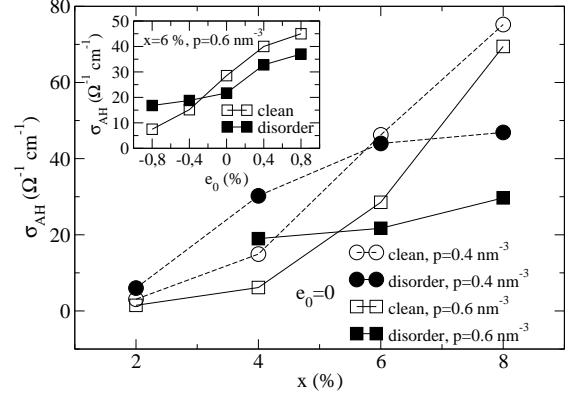


FIG. 4: Theoretical anomalous Hall conductivity of $\text{Mn}_x\text{Ga}_{1-x}\text{As}$ DMS calculated in the clean limit (open symbols) and accounting for the random distribution of Mn and As-antisite impurities (filled symbols), after Ref. 52.

A systematic comparison between theoretical and experimental AHE data is shown in Fig. 5.⁵² The results are plotted vs. nominal Mn concentration x while other parameters of the seven samples studied are listed in the figure legend. The measured σ_{AH} values are indicated by filled squares; triangles are theoretical results obtained in the clean limit or for a disordered system assuming either the As-antisite or Mn-interstitial compensation scenario. In general, when disorder is accounted for, the theory is in a good agreement with experimental data over the full range of studied Mn densities from $x = 1.5\%$ to $x = 8\%$. The effect of disorder, especially when assuming Mn-interstitial compensation, is particularly strong in the $x = 8\%$ sample shifting the theoretical σ_{AH} much closer to experiment compared to the clean limit theory. The remaining quantitative discrepancies between theory and experiment have been attributed to the resolution in measuring experimental hole and Mn densities.⁵²

We conclude this section by mentioning other studies of the anomalous Hall effect in regimes and geometries which we have not focused on here. A study within the non-metallic regime or hopping transport regime, not covered in any detailed within this review, has been done by Burkov *et al.*⁹⁷ following the ideas utilized in the metallic Berry's phase approach but generalized to hopping transport regime. Their results are in good agreement with experimental data in these regime which encompass samples with less than 1% doping. At temperatures above T_c , a theory based on semiclassical Boltzman transport has suggested the presence of anomalous Hall voltage noise within this regime which could be a further test of the intrinsic AHE model.⁹⁸

A recent theoretical study by Bruno *et al.*⁹⁹ has suggested an alternative experimental system to test the topological Hall effect arising from the Berry phase sim-

A. visible and infrared absorption

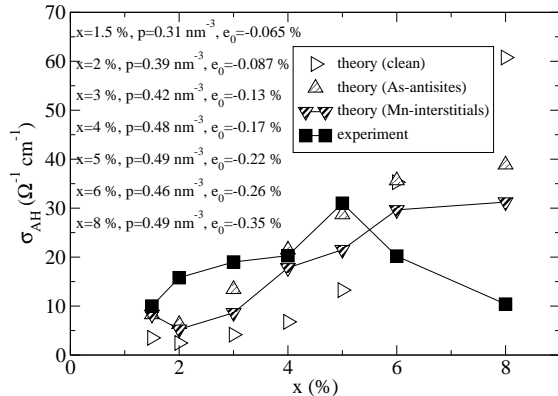


FIG. 5: Comparison between experimental and theoretical anomalous Hall conductivities, after Ref. 52.

ilar to Eq. 9. Here the difference is that the system has a spatially varying magnetization. Upon a local gauge transformation which makes the quantization axis oriented along the local magnetization direction, the problem becomes that of a gauge vector potential corresponding to monopole fields. Such a system can be created by sandwiching a thin film (II,Mn)VI semiconductor and a lattice of iron nano-rods oriented perpendicular to the doped semiconductor epilayer. Future experiments might show whether such a device can be grown efficiently and the theory tested.

IV. OPTICAL PROPERTIES OF DMS

Optical properties are among the key probes into the electronic structure of materials and, in the case of semiconductors, can also be utilized to change its properties by photo-carrier generation and other means. Given the wide energy range that optical probes can attain, many different physics can be addressed by exploring the full spectrum of phenomena including the visible and infrared absorption,^{31,100–105} magneto-optical effects such as the magnetic circular dichroism,^{31,106–108} Raman scattering,^{109–111} photoemission,^{22,23,112,113} and cyclotron resonance.^{114–116} We focus in this review on the first two items of this long list. The motivation for the study of optical properties of materials is two fold: first, it gives a consistency check on the different theoretical models and can be used to measure directly phenomenological parameters such as the exchange coupling J_{pd} ,^{107,108} and second, it can be utilized in applications such as magneto-optical memories, optical isolators, and circulators for optical communications.¹¹⁷

The simplest and most direct of the optical effects is light absorption, which probes the electronic structure through electron excitations between different bands or impurity states. An important measurement in semiconductors is the band edge absorption, usually obtained in the visible frequency range. This visible regime has been exploited more often using absorption from polarized light in order to measure magneto-optical effects such as the MCD and we will postpone its discussion to Sec. IV B. However, in the infrared regime, many of the meV physics is revealed and several remarkable experimental features have been observed in recent experiments.^{31,100,101,103–105} These experiments, performed in thin film geometries, exhibit several common phenomena: (i) a non-Drude behavior in which the conductivity increases with increasing frequency in the interval between 0 meV and 220 meV, (ii) a broad absorption peak near 220 – 260 meV that becomes stronger as the samples are cooled, and (iii) a broad featureless absorption between the peak energy and the effective band gap energy which tends to increase at the higher frequencies.

In order to understand these features, two theoretical approaches have been employed mostly. The first is the semi-phenomenological effective Hamiltonian model that focuses on the multi-band nature and on the intrinsic spin-orbit coupling present in the host semiconductor in order to quantitatively understand these materials and is able to capture many of the observed infrared properties.^{45,46,57} The second approach, used in the context of lattice models, emphasizes the connection with the localization physics present in the low doping regime and simplifies the electronic structure by assuming a single-band, seeking a more qualitative rather than quantitative understanding of these materials in the regime of interest. Both models are important to attain a full understanding of DMS optical properties and we review the results of each in turn.

1. Multiband effective Hamiltonian approach

Within the effective Hamiltonian model (Eq. 1), the 220 meV peak can be attributed to inter-valence-band transitions,⁴⁵ rather than to transitions between the semiconductor valence band states to a Mn induced impurity band, although a combination of these contributions will always be present. In thin film absorption measurements, for infrared wavelengths much larger than the width of the film, the real part of the conductivity is related to the absorption coefficient by

$$\tilde{\alpha}(\omega) = 2 \frac{\text{Re}[\sigma(\omega)]}{Y + Y_0}, \quad (15)$$

where Y and Y_0 are the admittances of the substrate and free space, respectively. For shorter wavelengths multiple reflections within the film must be taken into account

to obtain an estimate of the absorption coefficient. The conductivity tensor $\sigma_{\alpha,\beta}(\omega)$ at $T = 0$ can be evaluated using the standard Kubo formula for non-interacting quasiparticles. Disorder is taken into account within the Born approximation by including the lifetime broadening of quasiparticle spectral functions in evaluating the Kubo formula. The effective lifetime for transitions between bands n and n' , $\tau_{n,n'}$, is calculated by averaging quasiparticle scattering rates calculated from Fermi's golden rule including both screened Coulomb and exchange interactions as in Sec. III C. Fig. 6 shows the ac conductivities calculated for $\text{Ga}_{0.95}\text{Mn}_{0.05}\text{As}$ at a series of carrier densities.⁴⁵

An important concept in optical absorption spectra is the f-sum rule:

$$F \equiv \int_0^\infty d\omega \text{Re}[\sigma_{xx}(\omega)] = \frac{\pi e^2}{2V} \sum_\alpha f_\alpha \langle \alpha | \frac{\partial^2 H_{KL}}{\hbar^2 \partial k_x^2} | \alpha \rangle. \quad (16)$$

In this equation f_α is a quasiparticle Fermi factor and $\partial^2 H_{KL}/\hbar^2 \partial k_x^2$ is the xx component of the \mathbf{k}, \mathbf{p} model inverse effective mass operator. This sum rule is completely independent of the weak-scattering approximations but it is necessary to choose an upper cut-off for the frequency integral which creates a small uncertainty in the optical effective mass, defined by $F = \pi e^2 p / 2m_{opt}$. As illustrated in the inset of Fig 6, for the case of cut-off frequency $\hbar\omega_{max} = 800\text{meV}$, the f-sum rule values of F evaluated from our weak scattering theory are accurately linear in p over the entire range of relevant carrier densities. Disorder does have a small but measurable effect on m_{opt} as illustrated in Fig. 6. The optical masses for GaAs, InAs, and GaSb DMS ferromagnets with a 800, 400, and 700 meV cutoffs are 0.25-0.29 m_e , 0.40-0.43 m_e , and 0.21-0.23 m_e respectively, the extremes of these ranges corresponding to the clean (lower) and disordered (upper) limits of our model.⁴⁵

Free carrier concentration is difficult to determine accurately in DMS systems because the anomalous Hall contribution overwhelms the ordinary Hall coefficient and, in many instances, a high magnetic field is required. Hence, the f-sum rule can be used as an alternate tool to measure the free carrier concentration in metallic systems where the assumed electronic structure may be a good approximation so m_{opt} is given correctly by the estimates above. On the other hand, accurate estimates of the carrier concentration p can be used to test the theory as well. Recent experiments^{100,101} in as-grown samples have been interpreted in both ways without clear distinction between the effective Hamiltonian picture or the impurity band picture since no measurements of the carrier concentration were available. Further measurements in the most metallic samples will serve as test of the simplifying assumptions within this model.

One prominent feature that is at odds with experimental data from the above model calculations is the relative magnitude of the $\omega \rightarrow 0$ conductivity and the 220 meV conductivity peak. The reason is the impossibility of the

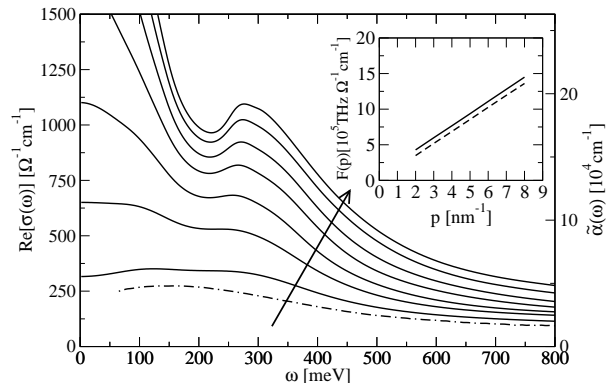


FIG. 6: Optical conductivity $\text{Re}[\sigma(\omega)]$ and absorption coefficient $\tilde{\alpha}(\omega)$ for carrier densities from $p = 0.2$ to 0.8nm^{-3} in the direction indicated by the arrow, for $\text{Ga}_{0.95}\text{Mn}_{0.05}\text{As}$. The dot-dashed line is an experimental absorption curve for a sample with a Mn concentration of 4% obtained from Ref. Hirakawa:2002. The inset shows the spectral weight $F(p)$ evaluated with a frequency cut-off of 800 meV including disorder (dashed) and in the clean limit (solid). After Ref. 45

model to account for weak and strong localization effects from multiple-scattering effects invariably present in the DMS materials and which suppress the low-frequency conductivity. Exact diagonalization calculations still within the effective Hamiltonian model in a finite system size but treating the disorder effects exactly can fix this shortcoming as shown in Fig. 7.⁴⁶ In this calculation the f-sum rule value differs from its Born approximation value by less than 10% for typical metallic carrier densities, hence justifying the use of m_{opt} as a measuring tool of the carrier concentration p .

2. Lattice models and dynamical mean field theory approach

Within the lattice models, dynamical mean-field-theory studies,^{118,119} for a single-band model that neglect the spin-orbit coupling and the heavy-light degeneracy of a III-V semiconductor valence band, have shown that non-Drude impurity-band related peaks in the frequency-dependent conductivity occur in DMS ferromagnet models when the strength of exchange interaction coupling is comparable to the band width. The starting Hamiltonian of these theories is the generalized Kondo lattice model

$$H = H_{host} - \sum_{i,\alpha,\beta} \mathbf{J}\hat{S}_i \cdot \psi_\alpha^\dagger(R_i) \vec{\sigma}_{\alpha\beta} \psi_\beta(R_i) + W \psi_\alpha^\dagger(R_i) \psi_\alpha(R_i), \quad (17)$$

where H_{host} describes carrier propagation in the host disordered semiconductor, here approximated by a single band Hamiltonian with semicircular density of states,

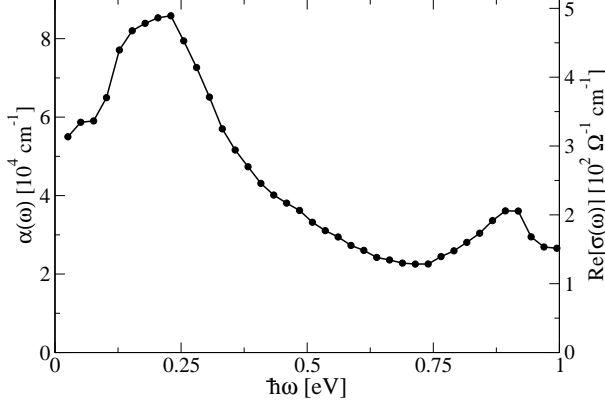


FIG. 7: Absorption and conductivity of a metallic sample computed using a Luttinger Kohn Hamiltonian with disorder. Here $p = 0.33 \text{ nm}^{-3}$, $n_{Mn} = 1 \text{ nm}^{-3}$ ($x \approx 4.5\%$). After Ref. 46

the second term describes the exchange coupling of the carriers to an array of Mn moments S_i at positions R_i , and the third term is the scalar part of the carrier-Mn potential.¹¹⁸ At zero temperature, when all Mn moments S_i are aligned, the carriers with spin parallel to S_i feel a potential $-J + W$ on each magnetic impurity site and anti-parallel carriers feel a potential $J + W$. Within this model, the disorder is treated in the dynamical mean field approximation, or equivalently in these systems the dynamical coherent potential approximation.¹²⁰ The real part of the conductivity is given by

$$\sigma(\Omega, T) = \int \frac{d^3p}{(2\pi)^3} \left(\frac{p \cos \theta}{m} \right)^2 \int \frac{d\omega}{\pi} \frac{[f(\omega) - f(\omega + \Omega)]}{\Omega} \times \text{Im}G(p, \omega) \text{Im}G(p, \omega + \Omega). \quad (18)$$

Typical results for the conductivity obtained within this model are shown in Fig. 3 of Ref. 118. Although the curves are similar to the ones obtained using the effective Hamiltonian multi-band models, the origin of the peak at intermediate frequencies is quite different. In the lattice model the peak corresponds to transitions between

the main band and the impurity band that forms when the carrier-Mn coupling becomes comparable or stronger to the main band width and spin-splitting. The high value of the exchange coupling required for this physics to apply is, however, not consistent with experimental J_{pd} values inferred from the visible-range MCD or magnetotransport measurements.^{5,108}

Monte Carlo simulations in closely related lattice models exhibit a similar conductivity behavior arising again from the presence of the impurity band.¹¹⁹ These theories point out the qualitative features present in the theoretical models as a function of the material parameters which, although fixed in most DMS materials, may be tuned by chemical engineering. It would be of interest to extend the calculation to a multi-band Hamiltonian model which may lead to a more complex description of the intermediate frequency regime. In addition, this extension would allow for a calculation of magneto-optical effects within this models which are not available at present.

B. Magneto-optical effects

Magneto-optical effects, such as magnetic circular dichroism (MCD), Kerr effect, and Faraday effect, give further insight in ferromagnetic materials and add an additional insight for the modeling of the electronic structure. Absorption and reflection measurements in the visible range have been used to establish phenomenological estimates for the p-d and s-d exchange coupling constants in DMS materials and are found to be in agreement with magnetic susceptibility measurements obtained from magneto-transport measurements in the paramagnetic regime.^{12,31,107,108} Measurements of magneto-optical coefficients on band energy scales provide very detailed information about the influence of broken time-reversal symmetry on itinerant electron quasiparticle states. For DMS materials the corresponding energy scale for the heavily p-doped (III,Mn)V ferromagnets is in the infrared. Within the effective Hamiltonian model, the anomalous Hall effect theory⁵² which has proven succesful when comparing closely with experimental results, can be easily extended to finite frequency range:⁵⁷

$$\text{Re}[\sigma_{xy}(\omega)] = -\frac{e^2 \hbar}{m^2 V} \frac{d\vec{k}}{(2\pi)^3} \sum_{\vec{k}n \neq n'} (f_{n',\vec{k}} - f_{n,\vec{k}}) \times \frac{\text{Im}[\langle n'\vec{k} | \hat{p}_x | n\vec{k} \rangle \langle n\vec{k} | \hat{p}_y | n'\vec{k} \rangle] (\Gamma_{n,n'}^2 + \omega(E_{n\vec{k}} - E_{n,\vec{k}'}) - (E_{n\vec{k}} - E_{n,\vec{k}'})^2)}{((\omega - E_{n\vec{k}} + E_{n,\vec{k}'})^2 + (\hbar\Gamma_{n,n'})^2)((E_{n\vec{k}} - E_{n,\vec{k}'})^2 + (\hbar\Gamma_{n,n'})^2)}, \quad (19)$$

where $\Gamma_{n,n'} \equiv (\Gamma_n + \Gamma_{n'})/2$ and Γ_n are the golden rule scattering rates averaged over band n as shown in Sec.

III C and IV A 1. Typical values for this anomalous ac-

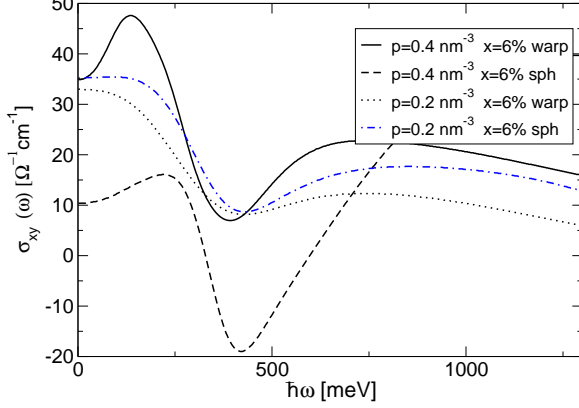


FIG. 8: Anomalous ac-Hall conductivity $\sigma_{xy}(\omega)$ for $x = 6\%$ Mn concentration and $p = 0.4$ and 0.2 nm^{-3} , for spherical and non-spherical (band-warping) models. After Ref. 57

Hall conductivity are shown in Fig. 8

The Hall conductivity σ_{xy} must be non-zero in order to have non-zero magneto-optical effects, such as the Faraday and Kerr effect, but the full conductivity tensor must be known in order to connect the calculations with the measurable quantities. The calculations and measurements mentioned here are for the Faraday geometry (magnetic field parallel to light propagation axis) for transmission and the polar Kerr geometry (near normal incidence with the magnetic field along the light propagation direction) for reflection. The complex Faraday angle $\tilde{\theta}_F$ includes both real and imaginary terms. $\tilde{\theta}_F$ is defined as

$$\tan \tilde{\theta}_F \equiv \frac{t_{xy}}{t_{xx}} = \frac{t_+ - t_-}{i(t_+ + t_-)} = \theta_F + i\eta_F, \quad (20)$$

where t_{xx} and t_{xy} are the complex transmission amplitudes for linearly polarized light and t_{\pm} are the total complex transmission amplitudes (with multiple scattering taken into account) for right and left circular polarized light. In typical measurements, $\tilde{\theta}_F$ is small and therefore the small angle approximation $\tan \tilde{\theta}_F \approx \tilde{\theta}_F$ can be used. The real term ($\text{Re}[\tilde{\theta}_F]$ or θ_F) corresponds to a simple geometric rotation of the polarization vector about the direction of propagation. The imaginary term ($\text{Im}[\tilde{\theta}_F]$ or η_F) relates directly to the ellipticity of the polarization. If the sample is axially symmetric along the magnetic field B , the transmittance tensor is diagonal when represented in the circular polarization basis. Therefore, changes in the incident polarization only depend on: (1) the relative difference in the phase of left versus right circularly polarized light due to $\text{Re}[\tilde{\theta}_F]$, which leads to a rotation (circular birefringence or Faraday rotation, FR) in the linearly polarized incident light; and (2) the relative difference in the transmission of left versus right circularly

polarized light due to $\text{Im}[\tilde{\theta}_F]$, which introduces ellipticity (circular dichroism, CD) to the linearly polarized incident light.

In the thin film approximation, the relationship between θ_F and the conductivity is given by:

$$\tan \theta_F \equiv \frac{t_{xy}}{t_{xx}} = \left(1 + \frac{1}{Z\sigma_{xx}}\right) \frac{\sigma_{xy}}{\sigma_{xx}} \quad (21)$$

where $Z = Z_0 d / (n+1)$, Z_0 is the impedance of free space, n is the substrate index of refraction, and d is the film thickness. In bulk, the angle of rotation per unit length traversed is

$$\theta_F(\omega) = \frac{4\pi}{(1+n)c} \text{Re}[\sigma_{xy}], \quad (22)$$

where c is the speed of light and n is the index of refraction of the substrate, in this case GaAs with $n = \sqrt{10.9}$.

CD or MCD (magnetic circular dichroism) is related to the difference between the optical absorption of right and left circularly polarized light, and is given by

$$MCD = \frac{\alpha^+ - \alpha^-}{\alpha^+ + \alpha^-} = \frac{\text{Im}[\sigma_{xy}(\omega)]}{\text{Re}[\sigma_{xx}(\omega)]} \propto \text{Im}[\tilde{\theta}_F]. \quad (23)$$

where α_{\pm} are the absorbances for left and right circularly polarized light. At visible range frequencies multiscattering reflections must be taken into account since in that regime the wavelength is comparable to the typical epilayer thickness.

Whereas the complex Faraday angle describes the polarization of a transmitted beam, the complex Kerr angle $\tilde{\theta}_K$ is applied in the same way for reflected radiation, with

$$\tan \tilde{\theta}_K \equiv \frac{r_{xy}}{r_{xx}} = \frac{r_+ - r_-}{i(r_+ + r_-)} = \theta_K + i\eta_K, \quad (24)$$

where r_{xx} and r_{xy} are the complex reflection amplitudes for linearly polarized light and r_{\pm} are the total complex reflection amplitudes (with multiple scattering taken into account) for right and left circular polarized light.

Fig. 9 shows the different magneto-optic effects predicted for a concentration of $x = 6\%$ and $p = 0.4 \text{ nm}^{-3}$. The Faraday rotation in this case is larger than the giant Faraday rotation observed in the paramagnetic (II,Mn)VI's at optical frequencies¹¹⁷ and should be readily observable in the highly metallic samples.

Though magneto-optical measurements on II-VI DMS materials have been extensive, see for example Ref. 121, measurements on III-V DMS have been more limited, with almost no Faraday/Kerr measurements reported on these compounds in the mid-infrared (MIR, 100-500 meV) range. The MIR range provides a critical test of the predictions in Ref. 45. Transmission and reflection MIR magneto-optic measurements on $\text{Ga}_{1-x}\text{Mn}_x\text{As}$ random alloy films in Figs. 10 and 11, respectively have been recently measured in this MIR range and support the presence of such strong magneto-optic signal in the MIR regime.¹²²

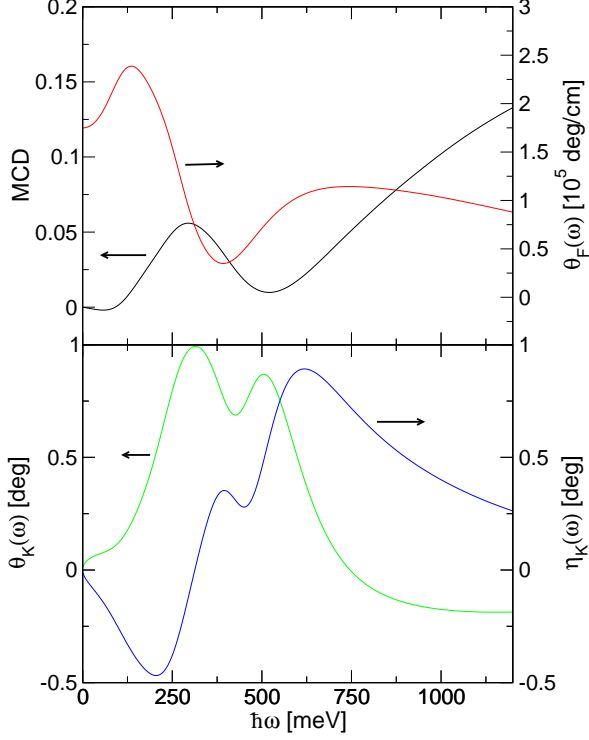


FIG. 9: Faraday and Kerr effects for $x = 6\%$ Mn concentration and $p = 0.4 \text{ nm}^{-3}$. After Ref. 57

Figure 10 plots the real a) and imaginary b) parts of the MIR $[\tilde{\theta}_F]$ probed at a photon energy of 118 meV and a sample temperature of 7 K. The hysteresis is weak and similar to out-of-plane dc magnetization measurements performed on this sample (a 6 % $\text{Ga}_{1-x}\text{Mn}_x\text{As}$ random alloy film). Both the real and imaginary parts of $[\tilde{\theta}_F]$ appear to be proportional to the film magnetization, as expected. The $\text{Re}[\tilde{\theta}_F]$ signal at magnetization saturation calculated by Sinova *et al.*⁴⁵ are on the order of 0.04 rad for a film with a similar thickness and Mn concentration. However such calculation are done in optimally annealed samples and further experimental measurements in this more metallic regime will be helpful to establish the validity of the model.

In Fig. 11, a two-step hysteresis loop is observed both the MIR (118 meV) $\text{Re}[\tilde{\theta}_K]$ as well as the dc magnetization for a 1 % $\text{Ga}_{1-x}\text{Mn}_x\text{As}$ random alloy film. This behavior is similar to that observed in MCD at a photon energy of 2.83 eV by Ref. 108. The authors in Ref. 108 claim that such behavior cannot be attributed to GaMn clusters, and therefore is a signature of the $\text{Ga}_{1-x}\text{Mn}_x\text{As}$ alloy.

The MIR magneto-optical measurement technique used in the above measurements is described in detail in Ref. 123, and results using this technique on non-magnetic systems are presented in Refs. 124 and 125. The results shown in Fig. 10 and 11 serve to demon-

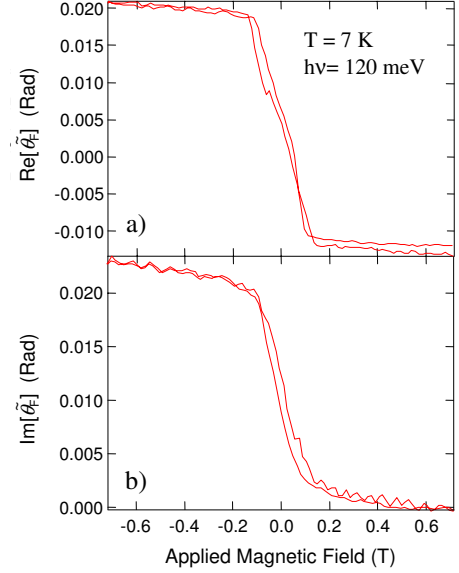


FIG. 10: $\text{Re}[\tilde{\theta}_F]$ a) and $\text{Im}[\tilde{\theta}_F]$ in the MIR range b) as a function of applied magnetic field for $\text{GaAs}(6 \text{ \% Mn})$ random alloy epilayer at 7 K and probe radiation energy 118 meV, after Ref. 122

strate the experimental feasibility of such studies, but further work is required to interpret these results and to compare them with theoretical predictions.

V. SUMMARY

This review has focused on highlighting the rapid developments in material research of metallic ferromagnetic (III,Mn)V semiconductors over the past few years. Although the successes have been extensive in the understanding and development of the bulk properties of the (Ga,Mn)As and (In,Mn)As systems within the metallic regime, many challenges remain both in other (III,Mn)V based semiconductors and lower dimensionalities such as digitally doped heterostructures. Both transport and magneto-optical effects will remain a very fruitful ground to make progress in these materials. At the time of writing, there is still a lot of work being done trying to sort out the more complicated physics of (Ga,Mn)N and several reports of high T_c measurements in the digitally doped materials. We simply keep watching in fascination the rapid developments and challenges posed by new

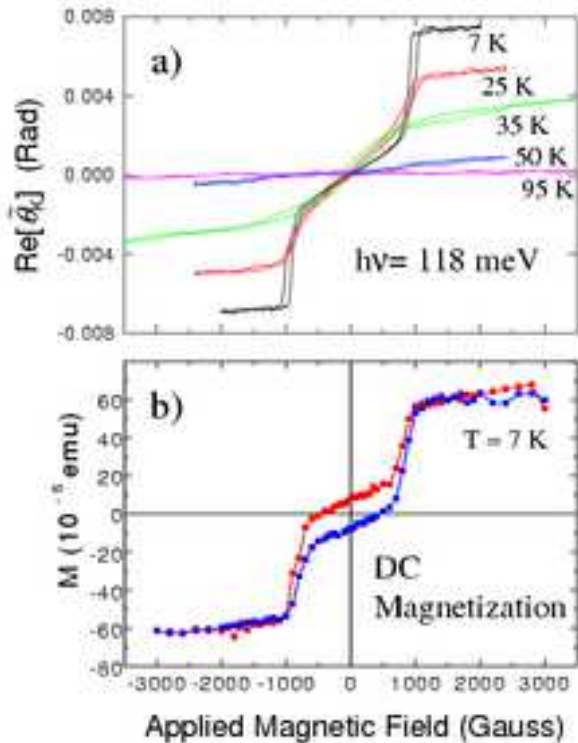


FIG. 11: $\text{Re}[\tilde{\theta}_K]$ in the MIR (118 meV) and dc magnetization (courtesy of S. Wang) for GaAs(1 % Mn) random alloy epilayer. After Ref. 122

experiments which will undoubtedly generate interesting physics and new understandings of these fascinating materials.

Acknowledgements

The many collaborators and colleagues with whom we have had the privilege to work with and learn from are too numerous to name here and we are grateful for their contribution to our knowledge of the subject. However, the authors would like to acknowledge insightful discussions during the course of this review with W. Atkinson, D. Basov, K. Burch, T. Dietl, J. Furdyna, H. Luo, J. Macek, A. H. MacDonald, B. McCombe, and C. Timm. This work was supported in part by the Welch Foundation, DOE under grant DE-FG03-02ER45958, and the Grant Agency of the Czech Republic under grant 202/02/0912.

- ¹ H. Ohno, H. Munekata, T. Penney, S. von Molnar, and L. L. Chang, *Phys. Rev. Lett.* **68**, 2664 (1992).
- ² H. Ohno, *Science* **281**, 951 (1998).
- ³ S. D. Sarma, E. H. Hwang, and A. Kaminski (2003), *cond-mat/0304219*.
- ⁴ C. Timm, *J. Phys.: Condensed Matter* **15**, R1865 (2003).
- ⁵ H. Ohno, *J. Magn. Magn. Mater.* **200**, 110 (1999).
- ⁶ T. Dietl, *Semicond. Sci. Technol.* **17**, 377 (2002).
- ⁷ F. Matsukura, H. Ohno, and T. Dietl, *Handbook of Magnetic Materials* **14**, 1 (2002).
- ⁸ J. König, J. Schliemann, T. Jungwirth, and A. MacDonald, in *Electronic Structure and Magnetism of Complex Materials*, edited by D. Singh and D. Papaconstantopoulos (Springer Verlag Berlin, 2003).
- ⁹ T. Dietl, H. Ohno, and F. Matsukura, *Phys. Rev. B* **63**, 195205 (2001).
- ¹⁰ S. Sanvito, G. Theurich, and N. Hill, *Journal of Superconductivity* **15**, 85 (2002).
- ¹¹ S. A. Wolf, D. D. Awschalom, R. A. Buhrman, J. M. Daughton, S. von Molnar, M. L. Roukes, A. Y. Chtchelkanova, and D. M. Treger, *Science* **294**, 1488 (2001).
- ¹² T. Dietl, *Acta Phys. Polon. A* **100**, 139 (2001).
- ¹³ J. F. Gregg, I. Petej, E. Jouguelet, and C. Dennis, *J. Phys. D: Appl. Phys.* **35**, R121 (2002).
- ¹⁴ H. Ohno, F. Matsukura, and Y. Ohno, *JSAP International* **5**, 4 (2002).
- ¹⁵ A. K. Bhattacharjee and C. B. La Guillaume, *Sol. State Comm.* **113**, 17 (2000).
- ¹⁶ M. Linnarsson, E. Janzén, B. Monemar, M. Kleverman, and A. Thilderkvist, *Phys. Rev. B* **55**, 6938 (1997).
- ¹⁷ J. Schneider, U. Kaufmann, W. Wilkening, M. Baeumler, and F. Kohl, *Phys. Rev. Lett.* **59**, 240 (1987).
- ¹⁸ S. C. Erwin and A. Petukhov, *Phys. Rev. Lett.* **89**, 227201 (2002).
- ¹⁹ J. Masek and F. Maca (2002), *cond-mat/0201131*.
- ²⁰ J. Szczytko, A. Twardowski, M. Palczewska, R. Jablonski, J. Furdyna, and H. Munekata, *Phys. Rev. B* **63**, 085315 (2001).
- ²¹ J. Szczytko, A. Twardowski, K. Swiatek, M. Palczewska, and K. A. M. Tanaka, T. Hayash, *Phys. Rev. B* **60**, 8304 (1999).
- ²² J. Okabayashi, A. Kimura, T. Mizokawa, A. Fujimori, T. Hayashi, and M. Tanaka, *Phys. Rev. B* **59**, R2486 (1999).
- ²³ J. Okabayashi, A. Kimura, O. Rader, T. Mizokawa, A. Fujimori, T. Hayashi, and M. Tanaka, *Phys. Rev. B* **64**, 125304 (2001).
- ²⁴ K. Edmonds, K. Wang, R. Champion, A. Neumann, N. Farley, B. Gallagher, and C. Foxon, *Appl. Phys. Lett.* **81**, 4991 (2002).
- ²⁵ K. C. Ku, S. J. Potashnik, R. F. Wang, M. J. Seong, E. Johnston-Halperin, R. C. Meyers, S. H. Chun, A. Mas-

- carenas, A. C. Gossard, D. D. Awschalom, et al., Appl. Phys. Lett. **82**, 2302 (2003).
- ²⁶ R. Mathieu, B. S. S rensen, J. Sadowski, J. Kanski, P. Svedlindh, and P. E. Lindelof (2002), cond-mat/0208411.
- ²⁷ K. M. Yu, W. Walukiewicz, T. Wojtowicz, I. Kuryliszyn, X. Liu, Y. Sasaki, , and J. K. Furdyna, Phys. Rev. B **65**, 201303 (2002).
- ²⁸ K. Edmonds, P. Boguslawski, K. Wang, R. Champion, N. Farley, B. Gallagher, C. Foxon, M. Sawicki, T. Dietl, M. Nardelli, et al., Phys. Rev. Lett. **92**, 037201 (2004).
- ²⁹ I.Kuryliszyn-Kudelska, T.Wojtowicz, X.Liu, J.K.Furdyna, W.Dobrowolski, J.Z.Domagala, E.Lusakowska, M.Goiran, E.Haanappel, and O. Portugall (2003).
- ³⁰ H. Ohno, D. Chiba, F. Matsukura, T. Omiya, E. Abe, T. Dietl, Y. Ohno, and K. Ohtani, Nature **408**, 944 (2000).
- ³¹ J. Szczytko, W. Mac, A. Twardowski, F. Matsukura, and H. Ohno, Phys. Rev. B **59**, 12935 (1999).
- ³² T. Omiya, F. Matsukura, T. Dietl, Y. Ohno, T. Sakon, M. Motokawa, and H. Ohno, Physica E **7**, 976 (2000).
- ³³ T. Dietl, Handbook of Semiconductors Vol. **3 B** (1994).
- ³⁴ J. Masek, J. Kudrnovsky, and F. Maca, Phys. Rev. B **67**, 153203 (2003).
- ³⁵ H. Akai, Phys. Rev. Lett. **81**, 3002 (1998).
- ³⁶ J. Park, S. Kwon, and B. Min, Physica B **281/282**, 703 (2000).
- ³⁷ J. Masek and F. Maca, Acta Phys. Polon. **A 102**, 667 (2002).
- ³⁸ J. Blinowski and P. Kacman, Phys. Rev. B **67**, 121204 (2003).
- ³⁹ T. Jungwirth, J. Masek, J. Sinova, and A. MacDonald, Phys. Rev. B **68**, 161202(R) (2003).
- ⁴⁰ R. Champion, K. Edmonds, L. Zhao, K. Wang, C. Foxon, B. Gallagher, and C. Staddon, J. Cryst. Growth **251**, 311 (2003).
- ⁴¹ R. N. Bhatt, M. Berciu, M. P. Kennett, and X. Wan, Journal of Superconductivity **15**, 71 (2002).
- ⁴² M. Abolfath, T. Jungwirth, J. Brum, and A. MacDonald, Phys. Rev. B **63**, 054418 (2001).
- ⁴³ I. Vurgaftman, J. Meyer, and L. Ram-Mohan, J. Appl. Phys **89**, 5815 (2001).
- ⁴⁴ T. Jungwirth, M. Abolfath, J. Sinova, J. Kucera, and A. MacDonald, Appl. Phys. Lett. **81**, 4029 (2002).
- ⁴⁵ J. Sinova, T. Jungwirth, S.-R. E. Yang, J. Kucera, and A. MacDonald, Phys. Rev. B **66**, 041202 (2002).
- ⁴⁶ S.-R. E. Yang, J. Sinova, T. Jungwirth, Y. Shim, and A. MacDonald, Phys. Rev. B **67**, 045205 (2003).
- ⁴⁷ J. Schliemann, Phys. Rev. B **67**, 045202 (2002).
- ⁴⁸ J. Schliemann and A. MacDonald, Phys. Rev. Lett. **88**, 137201 (2002).
- ⁴⁹ B. Lee, T. Jungwirth, and A. MacDonald, Semicond. Sci. Technol. **17**, 393 (2002).
- ⁵⁰ T. Dietl, H. Ohno, F. Matsukura, J. Cibert, and D. Ferrand, Science **287**, 1019 (2000).
- ⁵¹ T. Jungwirth, J. Konig, J. Sinova, J. Kucera, and A. MacDonald, Phys. Rev. B **66**, 012402 (2002).
- ⁵² T. Jungwirth, J. Sinova, K. Wang, K. W. Edmonds, R. Champion, B. Gallagher, C. Foxon, Q. Niu, and A. MacDonald, Appl. Phys. Lett. **83**, 320 (2003).
- ⁵³ T. Jungwirth, Q. Niu, and A. MacDonald, Phys. Rev. Lett. **88**, 207208 (2002).
- ⁵⁴ J. Konig, T. Jungwirth, and A. MacDonald, Phys. Rev. B **64**, 184423 (2001).
- ⁵⁵ T. Dietl, J. Konig, and A. H. MacDonald, Phys. Rev. B **64**, 241201 (2001).
- ⁵⁶ J. Sinova, T. Jungwirth, Y. S. X. Liu, J. Furdyna, W. A. Atkinson, and A. MacDonald (2003).
- ⁵⁷ J. Sinova, T. Jungwirth, J. Kucera, and A. MacDonald, Phys. Rev. B **67**, 235203 (2003).
- ⁵⁸ A. Chattopadhyay, S. D. Sarma, and A. J. Millis, Phys. Rev. Lett. **87**, 227202 (2001).
- ⁵⁹ F. Matsukura, H. Ohno, A. Shen, and Y. Sugawara, Phys. Rev. B **57**, R2037 (1998).
- ⁶⁰ S. J. Potashnik, K. C. Ku, S. H. Chun, R. F. Wang, M. B. Stone, N. Samarth, and P. Schiffer (2002), cond-mat /0212260.
- ⁶¹ A. V. Esch, L. V. Bockstal, J. D. Boeck, G. Verbanck, A. S. van Steenberghe, P. J. Wellmann, B. Grietens, R. B. F. Herlach, and G. Borghs, Phys. Rev. B **56**, 13103 (1997).
- ⁶² T. Hayashi, M. Tanaka, K. Seto, T. Nishinaga, and K. Ando, Appl. Phys. Lett. **71**, 1825 (1997).
- ⁶³ M. Lopez-Sancho and L. Brey, Phys. Rev. B **68**, 113201 (2003).
- ⁶⁴ S. J. Potashnik, K. C. Ku, R. Mahendiran, S. H. Chun, R. F. Wang, N. Samarth, and P. Schiffer, Phys. Rev. B **66**, 012408 (2002).
- ⁶⁵ D. V. Baxter, D. Ruzmetov, J. Scherschligt, Y. Sasaki, X. Liu, J. K. Furdyna, and C. H. Mielke, Phys. Rev. B **65**, 212407 (2002).
- ⁶⁶ K. W. Edmonds, R. P. Champion, K.-Y. Wang, A. C. Neumann, B. L. Gallagher, and P. C. M. C T Foxon, J. Appl. Phys. **93**, 6787 (2002).
- ⁶⁷ K. Wang, K. Edmonds, R. Champion, L. Zhao, A. Neumann, C. Foxon, B. Gallagher, and P. Main (2002), cond-mat/0211697.
- ⁶⁸ H. Tang, R. Kawakami, D. Awschalom, and M. Roukes, Phys. Rev. Lett. **90**, 107201 (2003).
- ⁶⁹ Sometimes it is called extraordinary or spin Hall effect, although these names are now in disuse and the later one is now used in a different context within paramagnetic materials.
- ⁷⁰ L. Chien and C. R. Westgate, *The Hall Effect and Its Applications* (Plenum, New York, 1980).
- ⁷¹ R. Karplus and J. Luttinger, Phys. Rev. **95**, 1154 (1954).
- ⁷² J. Smit, Physica **21**, 877 (1955).
- ⁷³ W. Kohn and J. Luttinger, Phys. Rev. **108**, 590 (1957).
- ⁷⁴ J. Luttinger, Phys. Rev. **112**, 739 (1958).
- ⁷⁵ E. Adams and E. Blount, J. Phys. Chem. Solids **10**, 286 (1959).
- ⁷⁶ L. Berger, Phys. Rev. B **2**, 4559 (1970).
- ⁷⁷ S. Lyo and T. Holstein, Phys. Rev. Lett. **29**, 423 (1972).
- ⁷⁸ P. Leroux-Hugon and A. Ghazali, J. Phys. C **5**, 1072 (1972).
- ⁷⁹ P. Nozieres and C. Lewiner, Le Journal de Physique **34**, 901 (1973).
- ⁸⁰ R. Fivaz, Phys. Rev. **183**, 586 (1969).
- ⁸¹ J. Chazalviel, Phys. Rev. B **11**, 3918 (1975).
- ⁸² T. Dietl, F. Matsukura, H. Ohno, J. Cibert, and D. Ferrand (2003), cond-mat/0306484.
- ⁸³ J. Smit, Phys. Rev. B **8**, 2349 (1973).
- ⁸⁴ L. Berger, Phys. Rev. B **8**, 2351 (1973).
- ⁸⁵ J. Smit, Phys. Rev. B **17**, 1450 (1978).
- ⁸⁶ L. Berger, Phys. Rev. B **17**, 1453 (1978).
- ⁸⁷ A. Crepieux and P. Bruno, Phys. Rev. B **64**, 014416 (2001).

- ⁸⁸ A. Crepieux and P. Bruno, Phys. Rev. B **64**, 094434 (2001).
- ⁸⁹ V. K. Dugaev, A. Crepieux, and P. Bruno, Phys. Rev. B **64**, 104411 (2001).
- ⁹⁰ M. Onoda and N. Nagaosa, J. Phys. Soc. Jap. **71**, 19 (2001).
- ⁹¹ Z. Fang, N. Nagaosa, K. S. Takahashi, A. Asamitsu, R. Mathieu, T. Ogasawara, H. Yamada, M. Kawasaki, Y. Tokura, and K. Terakura, Science **302**, 92 (2003).
- ⁹² Y. Taguchi, Y. Oohara, H. Yoshizawa, N. Nagaosa, and Y. Tokura, Science **291**, 2573 (2001).
- ⁹³ R. Shindou and N. Nagaosa, Phys. Rev. Lett. **87**, 116801 (2001).
- ⁹⁴ J. Ye, Y. b. Kim, A. J. Millis, B. I. Shraiman, P. Majumdar, and Z. Tesanovic, Phys. Rev. Lett. **83**, 3737 (1999).
- ⁹⁵ Y. Yao, L. Kleinman, A. H. MacDonald, J. Sinova, T. Jungwirth, D. sheng Wang, E. Wang, and Q. Niu, Phys. Rev. Lett. **86**, 037204 (2004).
- ⁹⁶ K. W. Edmonds, K. Y. Wang, R. P. Campion, A. C. Neumann, C. T. Foxon, B. L. Gallagher, and P. C. Main, Appl. Phys. Lett **81**, 3010 (2002).
- ⁹⁷ A. Burkov and L. Balents, Phys. Rev. Lett. **91**, 057202 (2003).
- ⁹⁸ C. Timm, F. von Oppen, and F. Holfing (2003), cond-mat/0309547.
- ⁹⁹ P. Bruno, V. K. Dugaev, and M. Taillefumier (2003), cond-mat/0310522.
- ¹⁰⁰ E. J. Singley, R. Kawakami, D. D. Awschalom, and D. N. Basov, Phys. Rev. Lett. **89**, 097203 (2002).
- ¹⁰¹ E. J. Singley, K. S. Burch, R. Kawakami, J. Stephens, D. D. Awschalom, and D. N. Basov, Phys. Rev. B **68**, 165204 (2003).
- ¹⁰² R. A. Chapman and W. G. Hutchinson, Phys. Rev. Lett. **18**, 443 (1967).
- ¹⁰³ K. Hirakawa, S. Katsumoto, T. Hayashi, Y. Hashimoto, and Y. Iye, Phys. Rev. B **65**, 193312 (2002).
- ¹⁰⁴ K. Hirakawa, A. Oiwa, and H. Munekata, Physica E **10**, 215 (2001).
- ¹⁰⁵ Y. Nagai, T. Kunimoto, K. Nagasaka, H. Nojiri, M. Motokawa, G. Matsukura, T. Dietl, and H. Ohno, Jpn. J. Appl. Phys. **40**, 6231 (2001).
- ¹⁰⁶ J. Szczytko, A. Stachow, W. Mac, A. Twardowski, P. Belca, and J. Tworzydło, Acta Physica Polonica **90**, 951 (1996).
- ¹⁰⁷ B. Beschoten, P. Crowell, I. Malajovich, and D. Awschalom, Phys. Rev. Lett. **83**, 3073 (1999).
- ¹⁰⁸ K. Ando, T. Hayashi, M. Tanaka, and A. Twardowski, J. Appl. Phys. **83**, 6548 (1998).
- ¹⁰⁹ M. J. Seong, S. H. Chun, H. M. Cheong, N. Samarth, and A. Mascarenhas, Phys. Rev. B **66**, 033202 (2002).
- ¹¹⁰ W. Limmer, M. Glunk, S. Mascheck, A. Koeder, W. Scoch, K. Thonke, R. Sauer, and A. Waag, Phys. Rev. B **66**, 205209 (2002).
- ¹¹¹ V. F. Sapega, T. Ruf, and M. Cardona, phs. stat. sol. b **226**, 339 (2001).
- ¹¹² J. Okabayashi, T. Mizokawa, D. D. Sarma, A. Fujimori, T. Slupinski, A. Oiwa, and H. Munekata, Phys. Rev. B **65**, 161203 (2002).
- ¹¹³ H. Asklund, L. Ilver, and J. S. J. Kanski, Phys. Rev. B **66**, 115319 (2002).
- ¹¹⁴ G. A. Khodaparast, J. Kono, Y. H. Matsuda, S. Ikeda, N. Miura, T. Slupinski, A. Oiwa, H. Munekata, Y. Sun, F. V. Kyrychenko, et al. (2003), cond-mat/0307087.
- ¹¹⁵ G. D. Sanders, Y. Sun, F. V. Kyrychenko, C. J. Stanton, G. A. Kodaparast, M. A. Zudov, J. Kono, N. M. Y. H. Matsuda, and H. Munekata (2003).
- ¹¹⁶ Y. Mitsumori, A. Oiwa, T. Slupinski, H. Maruki, Y. Kashimura, F. Minami, and H. Munekata (2003), cond-mat/0307268.
- ¹¹⁷ S. Sugano and N. Kojima, *Magneto-Optics* (Springer-Verlag, New York, 2000).
- ¹¹⁸ E. H. Hwang, A. J. Millis, and S. D. Sarma, Phys. Rev. B **65**, 233206 (2002).
- ¹¹⁹ G. Alvarez and E. Dagotto, Phys. Rev. B **68**, 045202 (2003).
- ¹²⁰ M. Takahashi (2003), cond-mat/0306588.
- ¹²¹ A. Ramdas and H. Alawadhi, Current Science **75**, 1216 (1998).
- ¹²² V. Patel, K. Smith, S.R. Cho, S. Wang, M. Cheong, H. Luo, A. Markelz, J. Černe, J. Sinova, X. Liu, Y. Sasaki, and J. Furdyna, to be published.
- ¹²³ J. Černe, D. Schmadel, L. Rigal, and H. Drew, Rev. Sci. Instr. **74**, 4755 (2003).
- ¹²⁴ J. Černe, M. Grayson, D. Schmadel, G. Jenkins, H. D. Drew, R. Hughes, J. Preston, , and P. Kung, Phys. Rev. Lett. **84**, 3418 (2000).
- ¹²⁵ J. Černe, D. Schmadel, M. Grayson, G. Jenkins, J. R. Simpson, and H. D. Drew, Phys. Rev. B **61**, 8133 (2000).